Build Simul (2020) 13: 709–727
https://doi.org/10.1007/s12273-020-0603-8

Coupling a goal-oriented inverse method and proper generalized decomposition for fast and robust prediction of quantities of interest in building thermal problems

Zohra Djatouti[1], Julien Waeytens[1] (✉), Ludovic Chamoin[2], Patrice Chatellier[1]

1. Université Paris-Est, IFSTTAR, 14-20 Bd Newton, 77447 Marne-La-Vallée Cedex 2, France
2. LMT-Cachan (ENS Paris-Saclay/CNRS/Université Paris-Saclay), 61 Avenue du Président Wilson, 94235 Cachan Cedex, France

Abstract

This article introduces a new inverse method for thermal model parameter identification that stands out from standard inverse methods by its formulation. While these latter methods aim at identifying all the model parameters in order to fit the experimental data at best, the proposed goal-oriented inverse method focuses on the prediction of a specific quantity of interest, automatically identifying and updating the model parameters involved in its computation alone. To further reduce the computational time, the goal-oriented inverse method is associated with a model order reduction method referred to as Proper Generalized Decomposition (PGD). The objective of this original approach is to robustly predict the sought quantity of interest in a reduced computational time while using a limited measurement data set. The goal-oriented inverse method is developed and illustrated on transient heat transfer models encountered in building thermal problems. The first application deals with a simplified 1D heat transfer problem through a building wall with synthetic data, and the second one is dedicated to a real building with measured data. The performance of the approach is numerically assessed by comparing the results with those obtained using the classical least squares method (with Tikhonov's regularization). It is shown that the goal-oriented inverse method allows to robustly predict the sought quantities of interest, with an error of less than 5% by updating only the model parameters that affect it the most and thus leads to save computation time compared to standard inversion methods.

Keywords

inverse problems,
quantity of interest,
goal-oriented strategy,
building thermal problems,
sensitivity analysis

Article History

Received: 08 April 2019
Revised: 18 December 2019
Accepted: 27 December 2019

1 Introduction

Mitigating the impact of the global warming is one of the critical current challenges. In this context, reducing buildings energy consumption is a major concern. Indeed, the building sector stands for more than 35% (IEA 2019) of the final energy consumption in the world. In France for instance, due to a low annual renewal rate of 1% to 2%, the building stock mainly consists of old and high energy-consuming buildings. Therefore, to achieve the target of the French government (−50% of final energy consumption by 2050), it is crucial to act on the existing buildings and important renovation works at the national level are necessary.

In order to choose the optimal renovation strategy, one needs to have a good knowledge of the buildings energy consumption and its distribution in the different energy consumption areas (heating, ventilation,...). Unfortunately, when it comes to old constructions, most of information required to estimate the real building consumption such as the building envelope composition are usually missing. Standardized methods are currently used to carry out building energy performance diagnosis. They are based on energy bills, with assumptions and mean values, so that results do not always reflect the real building behavior. There are also some non-destructive methods developed for onsite buildings characterization such as *ISABELE* method (Boisson and Bouchié 2014; Bouchié et al. 2014; Thébault and Bouchié 2018) and *QUB* (Alzetto et al. 2018; Mangematin et al. 2012) method, but these methods are only applicable in restrictive conditions (*e.g.*, they can only be used in unoccupied buildings).

To overcome the lack of effective tools in this field,

E-mail: julien.waeytens@ifsttar.fr

List of symbols

B_Q	thermal load of the adjoint problem related to thequantity of interest
$\mathbf{B}_Q$	nodal load vector associated with B_Q
C	global heat capacity ($J \cdot K^{-1}$)
h	convective heat exchange coefficient ($W \cdot m^{-2} \cdot K^{-1}$)
$\mathcal{J}$	minimization functional
k	global heat conduction coefficient ($W \cdot m^{-1} \cdot K^{-1}$)
L	thickness of the wall (m)
$\mathcal{L}$	Lagrangian
n_s	number of sensors
Q	quantity of interest
$\mathcal{Q}$	energy production inside the building (W)
q	heat flux ($W \cdot m^{-2}$)
$\mathcal{R}$	air renewal rate (s^{-1})
S_e	exchange surface area (m^2)
s	area of the envelope subjected to the solar heat flux (m^2)
T_i	temperature of the element specified by the index i (°C)
t	time coordinate (s)
U	thermal transmittance
$\mathcal{W}$	heating power (W)
x	space coordinate (m)
α/r	regularization parameters
τ	time constant of the envelope/building (s)
Γ_0	solar flux absorption coefficient of the outside wall surface
Φ	solar flux density ($W \cdot m^{-2}$)
$f(t)/h(x)$	time/space extractor functions
$B(t)/K(t)$	PGD time functions
$\mathbf{G}(\mathbf{x})/\mathbf{H}(\mathbf{x})$	PGD space functions
$\mathbf{P}(\mathbf{p})$	PGD parameter function

Indices

0/f	initial/final condition
a	air
mes	measured
out	outside environment
w/e	wall/envelope
wi/ei	inside wall/envelope surface
we/ee	outside wall/envelope surface
z	thermal zone
m	PGD mode number
M	PGD maximum number of modes

Matrix and vectors

$\mathbb{C}$	heat capacity matrix
$\mathbb{G}$	scaling matrix
$\mathbb{K}$	heat conduction matrix
$\mathbf{p}$	parameters vector
$\mathbf{\Gamma}$, $\mathbf{q}$	admissible fields introduced in the *mCRE* method
$\mathbf{T}$, $\mathbf{V}$, $\mathbf{W}$	temperature vectors (°C)
$\boldsymbol{\lambda}$, $\mathbf{\Lambda}$, $\boldsymbol{\gamma}$	Lagrange multipliers
$\mathbf{\Pi}$	extractor operator

inverse methods based on a combination of in situ measurements and numerical models can be used. Unlike the direct problem whose solution consists in finding the model response when its inputs are known, the solution of inverse problems consists in finding the model inputs knowing part of its response. Typically, solving a thermal inverse problem consists in finding the model parameters such as the material heat capacity and conductivity or the thermal sources knowing the temperature at some points. The major drawback of inverse problems is their ill-posed feature in the Hadamard sense (Hadamard 1923). On the one hand, the solution is generally not unique especially in thermal building problems where the number of sensors is small compared to the number of model parameters to be updated. On the other hand, the solution can be highly sensitive to data variations. To tackle these issues, different strategies are commonly implemented in building physics. First, a sensitivity analysis may be performed to evict the less sensitive model parameters from the updating process. As underlined in the review work (Rouchier 2018), local sensitivity analysis approaches are preferred to global sensitivity analysis approaches such as Morris and Sobol methods due to their lower computational cost. Some recent uses of sensitivity analysis for thermal building purposes can be found in (Berger et al. 2016b; Kristensen and Petersen 2016; Li et al. 2018; Martínez et al. 2019). Then, the inverse problem can be solved in deterministic or stochastic frameworks. In the deterministic context, inverse problems are formulated as minimization problems whose solution consists in finding the set of parameters for which the model solution best fits the measured data. Regularization methods such as the well-known Tikhonov method (Tikhonov and Arsenin 1977) are usually considered to prevent the solution to be sensitive to small sensor output perturbations. The regularization consists in adding to the minimization term (called the cost function) a second term (called the regularization term) that contains information constraining the solution to verify additional conditions. The Tikhonov method is a widespread regularization method, used for instance in (Artiges 2016; Brouns et al. 2016; Nassiopoulos et al. 2014). Let us note

that the computational cost of these standard deterministic inverse methods can drastically increase with the number of model parameters to be updated. In the stochastic context, Bayesian techniques are widely considered (Berger et al. 2016b; De Simon et al. 2018; Martínez et al. 2019; Raillon and Ghiaus 2018). In a preliminary stage, prior distribution for each model parameters has to be chosen which can be nontrivial. After a large number of computations for various sets of model inputs via Monte Carlo Markov Chain methods for example, model parameter posterior distributions are obtained. Thus, Bayesian techniques are usually more time consuming than deterministic inverse methods but model parameter confidence intervals can be derived from the posterior distributions. For more details on solving inverse problems in building physics, the reader can refer to the review article (Rouchier 2018).

The present paper deals with a goal-oriented inverse method introduced in (Chamoin et al. 2014) for mechanical problems. It is a variant of an alternative regularization method named "modified Constitutive Relation Error (*mCRE*)" (Ladevèze 1977) which is mainly used in mechanics. The *mCRE* concept was initially introduced in a global version to deal with nonlinear mechanics inverse problems (Chouaki et al. 1996; Ladevèze et al. 1994), *i.e.* data misfit minimization with a *mCRE* regularization term derived from the physics. The studied original goal-oriented identification method stands out from the standard global methods by its formulation that aims at predicting a predefined quantity of interest. It thus automatically identifies and updates model parameters involved in its computation alone, compared to standard inverse methods which identify all sensitive model parameters in order to accurately predict the full solution. The proposed approach naturally includes sensitivity analysis with respect to the quantity of interest, so that minimal model updating is performed to reach the targeted accuracy on the quantity of interest. In addition, it can be effectively used in the case of few measurement data. Contrary to mechanical problems, long time horizon are usually considered in building problems. In practice, this long time horizon can lead to memory issues when solving the original goal-oriented inverse method (Chamoin et al. 2014) due to coupled forward-backward thermal problems involved in its formulation. To tackle memory issues and to reduce the computational time, we propose herein to associate a model order reduction method in the inversion process. It refers to the Proper Generalized Decomposition (*PGD*) method (Chinesta et al. 2014) and is used here to decompose space and time variables. To summarize, the goal-oriented inverse method embedding a dedicated sensitivity analysis aims to accurately predict a quantity of interest by only updating the influential model parameters in a reduced computational time considering few sensors. For the first time, the overall inversion strategy combing the goal-oriented inverse method and the *PGD* is implemented and numerically analyzed on two transient heat transfer models encountered in building thermal problems. It is shown that it permits an accurate prediction of quantities of interest, for various configurations, with a fast and cheap process (few iterations) compared to classical approaches.

The paper is organized as follows: after this introduction, the considered framework of transient thermal model inversion is defined in Section 2; basics on the modified Constitutive Relation Error method, which is at the core of this work, are given in Section 3; the proposed goal-oriented inversion method is detailed in Section 4; the beneficial use of *PGD* model reduction is developed in Section 5; numerical results are reported in Section 6; eventually, conclusions and prospects are drawn in Section 7.

2 Inverse problems for building thermal applications

Building thermal problems are usually studied using models based on the partition of the building into thermal zones and walls (Hong and Jiang 1997). In such models, each thermal zone includes one or more rooms of the building where the temperature is homogeneous enough to be represented by a single point, whereas the walls describe the heat transfer between two adjacent zones or one zone and its adjacent environment. The thermal problem is then built by writing the heat transfer equations between each zone and its adjacent wall and through each wall. The simplest model of this type is the mono-zone model (Fig. 1) where the building is represented by one thermal zone and one wall. In this case, the problem is described by two equations: an ordinary differential equation for the heat transfer inside the thermal zone (1) and a partial differential equation for the heat transfer through the building wall (2). This procedure can be easily extended to more refined models including more thermal zones and walls. The model mono-zone reads:

$$\begin{cases} C_z \dfrac{\mathrm{d}T_z(t)}{\mathrm{d}t} = C_a \mathcal{R}\left(T_{out}(t) - T_z(t)\right) + h_i\left(T_{wi}(t) - T_z(t)\right) \\ \qquad\qquad + \Gamma_0 s\Phi(t) + \mathcal{W}(t) + \mathcal{Q}(t), \quad \forall t \in [0, t_f] \\ T_z(t=0) = T_{z_0} \end{cases} \tag{1}$$

$$\begin{cases} C_w \dfrac{\partial T_w}{\partial t}(x,t) - k_w \dfrac{\partial^2 T_w}{\partial x^2}(x,t) = 0, \quad \forall (x,t) \in]0, L[\times]0, t_f] \\ -k_w \dfrac{\partial T_w}{\partial t}(x=0,t) = q_0(t) + h_i\left(T_z(t) - T_{wi}(t)\right), \quad \forall t \in]0, t_f] \\ k_w \dfrac{\partial T_w}{\partial t}(x=L,t) = h_e\left(T_{out}(t) - T_{we}(t)\right), \quad \forall t \in]0, t_f] \\ T_w(x, t=0) = T_{w_0}(x), \quad \forall x \in [0, L] \end{cases} \tag{2}$$

where T_z (resp. T_w) denotes the room temperature (resp. wall

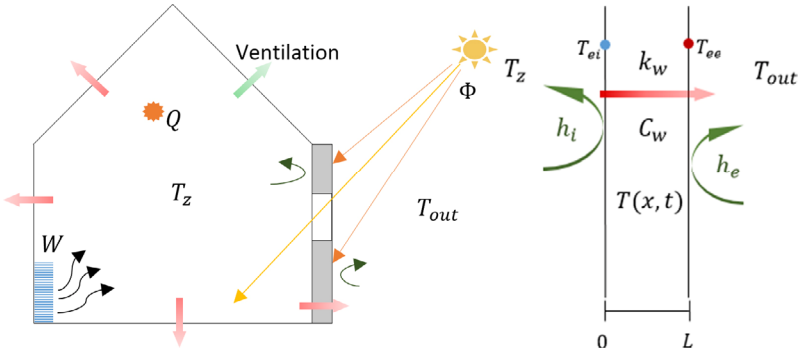

Fig. 1 A building mono-zone thermal model (left) and heat transfer through a building envelope (right)

temperature). The definition of the model parameters is given in the list of symbols.

For their numerical solution, Eqs. (1, 2) are expressed in a matrix form as:

$$\mathbb{C}\dot{\mathbf{T}} + \mathbb{K}\mathbf{T} = \mathbf{F} \tag{3}$$

The inverse problem associated with model parameter identification can be expressed as a least-square minimization problem that consists in finding the set of parameters $\mathbf{p}$ that minimizes the gap between the discretized simulated solution $\mathbf{T}$ of the problem (2) and the measurement data $\mathbf{T}_{\text{mes}}$. $\mathbf{T}_{\text{mes}}$ is a vector with n_s components where n_s is the number of temperature sensors. The problem reads:

$$\begin{aligned} \underline{\mathbf{p}} &= \arg\min_{\mathbf{p}} \mathcal{J}(\mathbf{T},\mathbf{p}) \\ \mathcal{J}(\mathbf{T},\mathbf{p}) &= \frac{1}{2}\int_0^{t_f} (\mathbf{T}_{\text{mes}} - \mathbf{\Pi T}(\mathbf{p}))^2 \mathrm{d}t \end{aligned} \tag{4}$$

where $\mathbf{\Pi}$ is an extraction operator. This type of problem is usually ill-posed in the sense of Hadamard (Hadamard 1923). To ensure the uniqueness of the solution, a priori information on the model parameters and regularization techniques such as the Tikhonov regularization technique (Tikhonov and Arsenin 1977) are often used. In the following, we focus on an alternative regularization technique based on the modified Constitutive Relation Error (*mCRE*) concept.

3 The modified Constitutive Relation Error method

For a better understanding of the goal-oriented inverse method, one should first introduce the modified Constitutive Relation Error (*mCRE*) method. The *mCRE* is a variational approach in which the regularization is based on the physics by imposing some admissibility constraints such as the equilibrium equations. The philosophy of the *mCRE* is to impose the most reliable information about the model (equilibrium, sensor position, ...) and to relax the less reliable ones (constitutive relations, measurement data, ...). The energy-based *mCRE* concept was initially introduced to deal with dynamic models in mechanics (Chouaki et al. 1996; Deraemaeker et al. 2002; Ladevèze et al. 1994, 1999), then it was successfully implemented in various applications including defects detection (Bui and Constanctinescu 2000), corrupted measurement data and uncertain models (Ladevèze and Pelle 2005; Ladevèze et al. 2006). It derives from the Constitutive Relation Error notion that has been used as an *a posteriori* discretization error control in finite element computations for more than 40 years (Ladevèze and Pelle 2005; Ladevèze and Chamoin 2015). The *mCRE* approach is based on a primal-dual formulation in a thermodynamic framework (Chavent et al. 1996) and involves a cost function with good convexity properties, even when dealing with nonlinear problems (Marchand et al. 2019). The use of the *mCRE* presents several advantages in the context of inverse problems: it was shown that the method is more robust to measurement noise and defective sensors than least-square based methods (Allix et al. 2005; Feissel and Allix 2007; Nguyen et al. 2008).

To illustrate the *mCRE* inversion method, we focus on the study of the heat transfer problem through a single building envelope described by Eq. (3). The *mCRE* framework leads to the following formulation: Find the trio $(T, \Gamma, \mathbf{q})$ such that:

- T is kinematically admissible; *i.e.* T satisfies the initial condition:

$$T = T_0, \quad \forall x \in [0,L], t = 0 \tag{5}$$

- $(\Gamma, \mathbf{q})$ is dynamically admissible; *i.e.* it verifies the equilibrium equations:

$$-\text{div}(\mathbf{q}) = \Gamma, \quad \forall x \in [0,L], t \in [0,t_f] \tag{6}$$

To use standard Finite Element methods, the admissible fields $\mathbf{q}$ and Γ are rewritten using additional temperature fields V and W such that:

$$\begin{cases} \mathbf{q} = -k\nabla V, & \forall x \in [0,L], t \in [0,t_f] \\ -\mathbf{q}\cdot\mathbf{n} = q_0 + h_i(V_z - V), & x = 0, t \in [0,t_f] \\ \mathbf{q}\cdot\mathbf{n} = h_e(V - T_{out}), & x = L, t \in [0,t_f] \end{cases} \tag{7}$$

and

$$\Gamma = C\frac{\partial W}{\partial t}, \quad \forall x \in [0,L], t \in [0,t_f] \tag{8}$$

Herein, replacing the fields $\mathbf{q}$ and Γ by their Eqs. (7, 8) in the weak form of (6) leads to:

$$\mathbb{C}\dot{\mathbf{W}} + \mathbb{K}\mathbf{V} = \mathbf{F} \tag{9}$$

Let us now introduce the cost function $\mathcal{J}_{CRE}$ which is associated with the inversion method based on the *CRE* concept, and referred to as the modified Constitutive Relation Error (*mCRE*). It reads:

$$\mathcal{J}_{CRE} = \frac{1}{2}\int_0^{t_f}\left\{(\mathbf{T}-\mathbf{V})^{\mathrm{T}}\mathbb{K}(\mathbf{T}-\mathbf{V}) + \left(\dot{\mathbf{T}}-\dot{\mathbf{W}}\right)^{\mathrm{T}}\tau\mathbb{C}\left(\dot{\mathbf{T}}-\dot{\mathbf{W}}\right)\right\}\mathrm{d}t + \frac{1}{2}\alpha\int_0^{t_f}(\mathbf{\Pi T}-\mathbf{T}_{\mathrm{mes}})^{\mathrm{T}}\mathbb{G}(\mathbf{\Pi T}-\mathbf{T}_{\mathrm{mes}})\mathrm{d}t \tag{10}$$

The first term of the cost function $\mathcal{J}_{CRE}$ measures the error on the constitutive relations (modeling error) while the second term is introduced to take into account the information provided by the measurement data (measurement error). This formulation implies two minimization steps: regarding the admissible fields and regarding the model parameters. $\mathbb{G}$ is a scaling diagonal matrix, τ is a characteristic time and α is the regularization coefficient. In practice α is chosen to give more or less weight to the model or the measurements ($\alpha \to 0$ means ∞that all the weight is given to the model, while $\alpha \to +\infty$ means that all the weight is given to the measurements). In the literature, this coefficient is usually taken equal to 1 so that neither the model, nor the data are privileged but some methods can be used to optimize the value of α such as the Morozov discrepancy principle (Morozov 1966) or the L-curve method (Lawson and Hanson 1974).

The thermal inverse problem consists then in finding the set of parameters that minimizes the cost function (10) among the admissible fields. This constrained minimization problem can be solved with an iterative gradient method and the adjoint-state method is used to computation of the gradient. For this purpose, we introduce the Lagrangian:

$$\mathcal{L}_{CRE} = \frac{1}{2}\int_0^{t_f}\left\{(\mathbf{T}-\mathbf{V})^{\mathrm{T}}\mathbb{K}(\mathbf{T}-\mathbf{V}) + \left(\dot{\mathbf{T}}-\dot{\mathbf{W}}\right)^{\mathrm{T}}\tau\mathbb{C}\left(\dot{\mathbf{T}}-\dot{\mathbf{W}}\right)\right\}\mathrm{d}t + \frac{1}{2}\alpha\int_0^{t_f}(\mathbf{\Pi T}-\mathbf{T}_{\mathrm{mes}})^{\mathrm{T}}\mathbb{G}(\mathbf{\Pi T}-\mathbf{T}_{\mathrm{mes}})\mathrm{d}t - \int_0^{t_f}\boldsymbol{\lambda}^{\mathrm{T}}\left(\mathbb{C}\dot{\mathbf{W}} + \mathbb{K}\mathbf{V} - \mathbf{F}\right)\mathrm{d}t \tag{11}$$

Finding its saddle point (12) leads to:

$$\begin{cases} \dfrac{\partial\mathcal{L}_{CRE}}{\partial\boldsymbol{\lambda}} = 0 \Rightarrow \mathbb{C}\dot{\mathbf{W}} + \mathbb{K}\mathbf{V} - \mathbf{F} = 0 \\ \dfrac{\partial\mathcal{L}_{CRE}}{\partial\mathbf{T}} = 0 \Rightarrow \mathbb{K}(\mathbf{T}-\mathbf{V}) - \tau\mathbb{C}\left(\ddot{\mathbf{T}}-\ddot{\mathbf{W}}\right) + \mathbf{\Pi}^{\mathrm{T}}\alpha\mathbb{G}(\mathbf{\Pi T}-\mathbf{T}_{\mathrm{mes}}) = 0 \\ \dfrac{\partial\mathcal{L}_{CRE}}{\partial\mathbf{V}} = 0 \Rightarrow \boldsymbol{\lambda} = (\mathbf{V}-\mathbf{T}) \\ \dfrac{\partial\mathcal{L}_{CRE}}{\partial\mathbf{W}} = 0 \Rightarrow \boldsymbol{\lambda} = \tau\left(\dot{\mathbf{W}}-\dot{\mathbf{T}}\right) \end{cases} \tag{12}$$

so that

$$\begin{bmatrix} \mathbb{C} & \mathbb{O} \\ \mathbb{O} & \mathbb{C} \end{bmatrix} \times \begin{Bmatrix} \dot{\mathbf{T}} \\ \dot{\boldsymbol{\lambda}} \end{Bmatrix} + \begin{bmatrix} \mathbb{K} & \frac{1}{\tau}\mathbb{C}+\mathbb{K} \\ \alpha\mathbf{\Pi}^{\mathrm{T}}\mathbb{G}\mathbf{\Pi} & -\mathbb{K} \end{bmatrix} \times \begin{Bmatrix} \mathbf{T} \\ \boldsymbol{\lambda} \end{Bmatrix} = \begin{Bmatrix} \boldsymbol{F} \\ \alpha\mathbf{\Pi}^{\mathrm{T}}\mathbb{G}\mathbf{T}_{\mathrm{mes}} \end{Bmatrix} \tag{13}$$

with

$$\begin{cases} \boldsymbol{\lambda} = (\mathbf{V}-\mathbf{T}) \\ \boldsymbol{\lambda} = \tau\left(\dot{\mathbf{W}}-\dot{\mathbf{T}}\right) \end{cases} \tag{14}$$

and

$$\begin{cases} \mathbf{T} = \mathbf{T}_0, & \forall x \in [0,L], t = 0 \\ \boldsymbol{\lambda} = 0, & \forall x \in [0,L], t = t_f \end{cases} \tag{15}$$

The system (13–15) is a coupled forward-backward problem since the temperature field $\mathbf{T}$ has a known initial condition while the Lagrange multiplier $\boldsymbol{\lambda}$ has a known final condition. The field $\mathbf{T}$ satisfying the system (13–15) can be seen as an extrapolation of the measured data using the numerical model. Let us notice that the measurement data are not taken into account as imposed temperatures but are considered through a penalization term.

4 Goal-oriented inverse method

The goal-oriented inverse method introduced in (Chamoin et al. 2014) derives from the *mCRE* regularization method (Chouaki et al. 1996; Ladevèze et al. 1994). Unlike the standard inverse methods such as the Tikhonov (Tikhonov and Arsenin1977) and the *mCRE* methods which aim at identifying all the model parameters in order to compute the solution of the physical problem, the goal-oriented inverse method focuses on the robust prediction of a scalar quantity of interest, and thus aims at identifying only the set of parameters involved in its computation. This strategy is similar to the approach used in (Becker and Vexler 2004) and (Johansson et al. 2011) where the model and the discretization errors were controlled to predict a quantity of interest. The sought quantity of interest can be any output of the studied model such as the temperature evolution at a

given position in the building or the energy loss through an envelope wall during a given period of time. Once the quantity of interest Q is chosen, the cost function is expressed to minimize the gap between the quantity of interest calculated from two different ways: Q_1 is computed from the direct solution $\mathbf{T}_1$ of the numerical model while Q_2 is obtained with the temperature field $\mathbf{T}_2$ calculated by an extrapolation of the measured data with the numerical model:

$$\mathcal{J}_Q(\mathbf{T},\mathbf{p}) = \frac{1}{2} r[Q_1(\mathbf{T}_1(\mathbf{p})) - Q_2(\mathbf{T}_2(\mathbf{p}))]^2 \tag{16}$$

where $r = \alpha/(1+\alpha)$, α being the regularization parameter and $\mathbf{T}_2$ derives from the *mCRE* framework (see Eqs. (13–15)). In practice, the coefficient α involved in the r term of the goal-oriented inverse functional is the same as the α introduced in the modified Constitutive Relation Error functional (see Eq. 10).

This minimization problem is solved using a gradient method where the descent direction is determined using the adjoint state method (see Section 3). We then introduce the Lagrangian $\mathcal{L}_Q$:

$$\begin{aligned}\mathcal{L}_Q(\mathbf{T},\boldsymbol{\Lambda},\mathbf{p}) = {} & \frac{1}{2} r[Q_1(\mathbf{T}_1(\mathbf{p})) - Q_2(\mathbf{T}_2(\mathbf{p})]^2 \\ & - \int_0^{t_f} \boldsymbol{\Lambda}_1^{\mathrm{T}} \left[\mathbb{C}\dot{\mathbf{T}}_1 + \mathbb{K}\mathbf{T}_1 - \mathbf{F} \right] \mathrm{d}t \\ & - \int_0^{t_f} \boldsymbol{\Lambda}_2^{\mathrm{T}} \left[\mathbb{C}\dot{\mathbf{T}}_2 + \mathbb{K}\mathbf{T}_2 + \left(\frac{1}{\tau}\mathbb{C} + \mathbb{K}\right)\boldsymbol{\lambda}_2 - \mathbf{F} \right] \mathrm{d}t \\ & - \int_0^{t_f} \boldsymbol{\gamma}_2^{\mathrm{T}} \left[\mathbb{C}\dot{\boldsymbol{\lambda}}_2 + \alpha\boldsymbol{\Pi}^{\mathrm{T}}\mathbb{G}\boldsymbol{\Pi}\mathbf{T}_2 - \mathbb{K}\boldsymbol{\lambda}_2 - \alpha\boldsymbol{\Pi}^{\mathrm{T}}\mathbb{G}\mathbf{T}_{\mathrm{mes}} \right] \mathrm{d}t \end{aligned} \tag{17}$$

Finding the saddle point of (17) leads to solve Eq. (18).

$$\begin{cases} \dfrac{\partial \mathcal{L}_Q}{\partial \mathbf{T}_1} = 0 \Leftrightarrow \mathbb{C}\dot{\boldsymbol{\Lambda}}_1 - \mathbb{K}\boldsymbol{\Lambda}_1 = -\mathbf{B}_Q \\ \dfrac{\partial \mathcal{L}_Q}{\partial \mathbf{T}_2} = 0 \Leftrightarrow \mathbb{C}\dot{\boldsymbol{\Lambda}}_2 - \mathbb{K}\boldsymbol{\Lambda}_2 - \alpha\boldsymbol{\Pi}^{\mathrm{T}}\mathbb{G}\boldsymbol{\Pi}\boldsymbol{\gamma}_2 = \mathbf{B}_Q \\ \dfrac{\partial \mathcal{L}_Q}{\partial \boldsymbol{\lambda}_2} = 0 \Leftrightarrow \mathbb{C}\dot{\boldsymbol{\gamma}}_2 + \mathbb{K}\boldsymbol{\gamma}_2 - \left(\dfrac{1}{\tau}\mathbb{C} + \mathbb{K}\right)\boldsymbol{\Lambda}_2 = 0 \\ \dfrac{\partial \mathcal{L}_Q}{\partial \boldsymbol{\Lambda}_1} = 0 \Leftrightarrow \mathbb{C}\dot{\mathbf{T}}_1 + \mathbb{K}\mathbf{T}_1 = \mathbf{F} \\ \dfrac{\partial \mathcal{L}_Q}{\partial \boldsymbol{\Lambda}_2} = 0 \Leftrightarrow \mathbb{C}\dot{\mathbf{T}}_2 + \mathbb{K}\mathbf{T}_2 + \left(\dfrac{1}{\tau}\mathbb{C} + \mathbb{K}\right)\boldsymbol{\lambda}_2 = \mathbf{F} \\ \dfrac{\partial \mathcal{L}_Q}{\partial \boldsymbol{\gamma}_2} = 0 \Leftrightarrow \mathbb{C}\dot{\boldsymbol{\lambda}}_2 + \alpha\boldsymbol{\Pi}^{\mathrm{T}}\mathbb{G}\boldsymbol{\Pi}\mathbf{T}_2 - \mathbb{K}\boldsymbol{\lambda}_2 = \alpha\boldsymbol{\Pi}^{\mathrm{T}}\mathbb{G}\mathbf{T}_{\mathrm{mes}} \end{cases} \tag{18}$$

Rewriting these equations in a concatenated form (19) leads to solve four problems: the first one is the direct heat transfer problem, the second one is an adjoint problem and the third and the fourth ones are two forward/backward problems leading to the computation of the temperature vector $\mathbf{T}_2$ by extrapolating the measured data through the model and the Lagrange multipliers $\boldsymbol{\Lambda}_2$, $\boldsymbol{\lambda}_2$ and $\boldsymbol{\gamma}_2$ that will be used for the computation of the gradient of the functional $\mathcal{J}_Q$ with respect to the model parameters.

$$\begin{cases} \mathbb{C}\dot{\mathbf{T}}_1 + \mathbb{K}\mathbf{T}_1 = \mathbf{F} \\ \mathbb{C}\dot{\boldsymbol{\Lambda}}_1 - \mathbb{K}\boldsymbol{\Lambda}_1 = -\mathbf{B}_Q \\ \begin{bmatrix} \mathbb{C} & \mathbb{O} \\ \mathbb{O} & \mathbb{C} \end{bmatrix} \times \begin{Bmatrix} \dot{\mathbf{T}}_2 \\ \dot{\boldsymbol{\lambda}}_2 \end{Bmatrix} + \begin{bmatrix} \mathbb{K} & \frac{1}{\tau}\mathbb{C} + \mathbb{K} \\ \alpha\boldsymbol{\Pi}^{\mathrm{T}}\mathbb{G}\boldsymbol{\Pi} & -\mathbb{K} \end{bmatrix} \times \begin{Bmatrix} \mathbf{T}_2 \\ \boldsymbol{\lambda}_2 \end{Bmatrix} = \begin{Bmatrix} \mathbf{F} \\ \alpha\boldsymbol{\Pi}^{\mathrm{T}}\mathbb{G}\mathbf{T}_{\mathrm{mes}} \end{Bmatrix} \\ \begin{bmatrix} \mathbb{C} & \mathbb{O} \\ \mathbb{O} & \mathbb{C} \end{bmatrix} \times \begin{Bmatrix} \dot{\boldsymbol{\gamma}}_2 \\ \dot{\boldsymbol{\Lambda}}_2 \end{Bmatrix} + \begin{bmatrix} \mathbb{K} & -\frac{1}{\tau}\mathbb{C} - \mathbb{K} \\ -\alpha\boldsymbol{\Pi}^{\mathrm{T}}\mathbb{G}\boldsymbol{\Pi} & -\mathbb{K} \end{bmatrix} \times \begin{Bmatrix} \boldsymbol{\gamma}_2 \\ \boldsymbol{\Lambda}_2 \end{Bmatrix} = \begin{Bmatrix} 0 \\ \mathbf{B}_Q \end{Bmatrix} \end{cases} \tag{19}$$

with

$$\begin{cases} \mathbf{T}_1 = \mathbf{T}_0, & \forall x \in [0,L], t = 0 \\ \boldsymbol{\Lambda}_1 = 0, & \forall x \in [0,L], t = t_f \\ \mathbf{T}_2 = \mathbf{T}_0, & \forall x \in [0,L], t = 0 \\ \boldsymbol{\lambda}_2 = \mathbf{V}_2 - \mathbf{T}_2, & \forall (x,t) \in [0,L] \times [0,t_f] \\ \boldsymbol{\lambda}_2 = 0, & \forall x \in [0,L], t = t_f \\ \boldsymbol{\gamma}_2 = 0, & \forall x \in [0,L], t = 0 \\ \boldsymbol{\Lambda}_2 = 0, & \forall x \in [0,L], t = t_f \end{cases} \tag{20}$$

$\mathbf{B}_Q$ is a nodal force vector associated with $B_Q(x, t)$ defined by:

$$B_Q(x,t) = r[Q_1 - Q_2] \frac{\partial Q}{\partial T} \tag{21}$$

and the quantity of interest Q is rewritten using an extractor function in space $h(x)$ and extractor function in time $f(t)$

$$Q(T) = \int_0^{t_f} \int_0^L T(x,t) f(t) h(x) \mathrm{d}x \mathrm{d}t \tag{22}$$

Hence

$$\frac{\partial Q}{\partial T} \delta T = \int_0^{t_f} \int_0^L \delta T f(t) h(x) \mathrm{d}x \mathrm{d}t \tag{23}$$

$$B_Q(x,t) = r[Q_1 - Q_2] f(t) h(x) \tag{24}$$

To sum up, solving the inverse problem of model parameter identification using the goal-oriented inverse method consists of repeating the following steps:

1) Solve the direct heat transfer equation (first equation in (19)) in order to compute the temperature vector $\mathbf{T}_1$ and the quantity of interest Q_1.

2) Solve the first coupled forward/backward problem (third equation in (19)) in order to compute the temperature vector $\mathbf{T}_2$, the Lagrange multiplier $\boldsymbol{\lambda}_2$ and the quantity of interest Q_2.
3) Solve the second coupled forward/backward problem (forth equation in (19)) in order to compute the Lagrange multipliers $\boldsymbol{\Lambda}_2$ and $\boldsymbol{\gamma}_2$.
4) Solve the adjoint problem (second equation in (19)) in order to compute the Lagrange multiplier $\boldsymbol{\Lambda}_1$.
5) Compute the gradient $\nabla_{\mathbf{p}}\mathcal{J}_Q$ then determine the descent direction and select the parameter to be updated. Only the parameter leading to the highest value of the gradient is updated.
6) Evaluate the functional $\mathcal{J}_Q$ (16).

Remark 1

Step 5 indicates how the model parameter to be updated is selected at each iteration. This procedure can be seen as an alternative to the standard sensitivity analysis methods (Kleiber et al. 1997; Saltelli et al. 2000). Indeed, when there is a large number of unknown parameters, a sensitivity analysis is usually used to determine the most influential parameters and update them, while the less influential ones are fixed at their nominal values (Heiselberg et al. 2007; Gagnon et al. 2018). These methods can be expensive in terms of computation time and lead to rank the parameters into influential and less influential without taking into account whether they are well identified or not. Even after choosing a dimensionless framework, and using homogenization and engineering experience on the model, it is still possible to end up with parameters that only have marginal influence on the quantity of interest for the design problem considered. This can be highlighted using global sensitivity analysis (GSA) or Sobol indices. The proposed method simultaneously and automatically includes sensitivity of parameters with respect to the quantity of interest, and measurement sensitivity with respect to parameters.

Remark 2

On the one hand the solution of the thermal inverse problem usually requires a long observation period, on the other hand the updating process of the goal-oriented inverse method requires to solve two coupled forward-backward thermal problems at each iteration. This can lead to high dimensional numerical problems ($2N_x \times N_t$, where N_x is the space dimension and N_t the time dimension), and thus be computationally prohibitive. To tackle memory issues and to decrease the computation cost, several techniques can be used. We propose herein to use the Proper Generalized Decomposition (*PGD*) model reduction method, which is introduced in the next section. The use of the PGD for inverse problems was investigated in many application areas such as geophysics, structural mechanics and thermal building problems (Berger et al. 2016a, 2017a,b; Beringhier and Gigliotti 2015; Bouclier et al. 2013; González et al. 2012; Marchand and Chamoin 2016; Rubio et al. 2018; Signorini et al. 2017).

5 PGD model reduction method

To override the computational time and the memory storage constraints due to the multiple resolutions of the two coupled forward-backward problems (third and fourth equations in (19)) during the updating procedure, one can resort to Reduced Order Methods (*ROM*) (Chinesta et al. 2004; Rozza et al. 2018). Among the various reduced order methods available in the literature, we can cite the Proper Orthogonal Decomposition (*POD*) method (Chatterjee 2000), the Singular Value Decomposition (*SVD*) method (Golub and Reinsch 1970; Klema and Laub 1980), and Reduced Basis methods (*RB*) (Ohlberger and Rave 2016; Quarteroni et al. 2016; Rozza 2009). These model order reduction methods, based on the approximation of large size systems with much smaller systems, lead to an optimization of the numerical capabilities and a considerable computation time shortening without compromising the precision. Sometimes called *a posteriori* methods, they require a prior information collection and their results are often exploitable only in similar conditions to those where information were collected. Another group of methods, called *a priori* methods because their construction does not require any information and is only based on the problem equations, is the Proper Generalized Decomposition (*PGD*) method, introduced in (Allix et al. 1989) under the denomination "Radial time-space approximation". The *PGD* method was initially introduced to tackle nonlinear mechanics problems as mechanical damage and was used in combination with the *LATIN* (*LArge Time INcrement*) method (Ladevèze and Chouaki 1999) then extended to various applications in different aspects of solid and fluid mechanics (Chinesta et al. 2011). The Proper Generalized Decomposition relies on the variable separability of the problem equations. It allows the calculation of a given field (temperature field in our case) as a superposition of a finite number of approximate solutions written as a product of two or more functions, called modes. Each mode is a product of functions of a single variable that can be the time, the space or any model parameter (25).

$$T(x,t,\mathbf{p}) = \sum_{n=1}^{M} \mathbf{G}_n \times B_n(t) \times P_n(\mathbf{p}) \tag{25}$$

where $\mathbf{G}_n$ are the space modes, $B_n(t)$ the time modes, $P_n(\mathbf{p})$

the parameter modes, and M the number of modes. The fundamentals and the formulation of the *PGD* method on the solution of partial differential equations are given in (Nouy 2010). The possibility of expressing explicitly the problem equations with regard to the model parameters is of a great interest in the case of model parameter identification problems. Indeed, during the identification process, the *PGD* solution is computed only once and the same solution is used to adjust the model parameters during the whole updating process. Some examples of the use of the *PGD* method in combination with the *mCRE* can be found in the literature (Bouclier et al. 2013; Marchand and Chamoin 2016). When the *PGD* method is applied in combination with the *mCRE* method, the reduced basis is built from the data. This approach is similar to the *GEIM* and *PBDW* strategies used in (Maday and Mula 2013; Maday et al. 2015a,b), and is equivalent to the methods used in (Becker and Vexler 2004) and (Johansson et al. 2007) but is different from the classical model calibration approaches using the *PGD* such as (González et al. 2012). The *PGD* method can also be exploited as an alternative to the sensitivity-based approaches used in (Alekseev and Navon 2010; Daescu and Carmichael 2003; Kleiber et al. 1997; Waeytens et al. 2017) or to the energetic considerations in (Papadimitriou and Lombaert 2012) to optimize the number of sensors required for the model calibration. This can be achieved if the sensors are placed at the positions where the space modes amplitudes are the largest. A similar strategy, based on the reduced basis method, is adopted in (Maday et al. 2015a) and (Binev et al. 2018).

In this work, the *PGD* method is mainly used as an alternative to the *Ricatti* approaches (Nguyen et al. 2008) or temporal scheme based methods (Bonnet and Wilkins 2014) to reduce the computation time due to the coupled forward-backward problems (see Eq. (19)) by separating the time and space variables alone, similarly to what is done in (Marchand et al. 2016).

5.1 Solution of the coupled problems using the PGD method

The first forward/backward problem

We first deal with the forward/backward problem expressed by the third equation in (19). To make the notation less cluttered, the index 2 is omitted on purpose. We first replace the vectors $\mathbf{T}$ and $\boldsymbol{\lambda}$ by their separated form $\mathbf{T}_m$ and $\boldsymbol{\lambda}_m$, expressed in (26) where $\mathbf{G}_m$ and $\tilde{\mathbf{G}}_m$, $B_m(t)$ and $\tilde{B}_m(t)$ depend respectively on space and time variables. We introduce a Galerkin formulation in the tangent space by multiplying the equation by two test fields $\delta\mathbf{T}_m$ and $\delta\boldsymbol{\lambda}_m$ (27) and we obtain (28).

$$\begin{cases} \mathbf{T}_m = \sum_{n=1}^{m} \mathbf{G}_n \times B_n(t) \\ \boldsymbol{\lambda}_m = \sum_{n=1}^{m} \tilde{\mathbf{G}}_n \times \tilde{B}_n(t) \end{cases} \tag{26}$$

$$\begin{cases} \delta\mathbf{T}_m = \delta\mathbf{G}_m B_m(t) + \mathbf{G}_m \delta B_m(t) \\ \delta\boldsymbol{\lambda}_m = \delta\tilde{\mathbf{G}}_m \tilde{B}_m(t) + \tilde{\mathbf{G}}_m \delta\tilde{B}_m(t) \end{cases} \tag{27}$$

$$\begin{Bmatrix} \delta\mathbf{T}_m \\ \delta\boldsymbol{\lambda}_m \end{Bmatrix}^{\mathrm{T}} \times \left\{ \begin{bmatrix} \mathbb{C} & \mathbb{O} \\ \mathbb{O} & \mathbb{C} \end{bmatrix} \times \begin{Bmatrix} \dot{\mathbf{T}}_m \\ \dot{\boldsymbol{\lambda}}_m \end{Bmatrix} + \begin{bmatrix} \mathbb{K} & \frac{1}{\tau}\mathbb{C} + \mathbb{K} \\ \alpha\boldsymbol{\Pi}^T \mathbb{G} \boldsymbol{\Pi} & -\mathbb{K} \end{bmatrix} \times \begin{Bmatrix} \mathbf{T}_m \\ \boldsymbol{\lambda}_m \end{Bmatrix} - \begin{Bmatrix} \mathbf{F} \\ \alpha\boldsymbol{\Pi}^T \mathbb{G} \mathbf{T}_{\mathrm{mes}} \end{Bmatrix} \right\} = 0 \tag{28}$$

Solving (28) leads to solve two systems (29) and (30), leading respectively to the computation of the space modes $\mathbf{G}_m$ and $\tilde{\mathbf{G}}_m$ and the time modes $B_m(t)$ and $\tilde{B}_m(t)$. Let us notice that these two systems are coupled and a fixed point algorithm is therefore used to solve them.

$$\begin{bmatrix} k_{G_1} & k_{G_2} \\ k_{G_3} & k_{G_4} \end{bmatrix} \times \begin{Bmatrix} \mathbf{G}_m \\ \tilde{\mathbf{G}}_m \end{Bmatrix} = \begin{Bmatrix} f_{G_1} \\ f_{G_2} \end{Bmatrix} \tag{29}$$

$$\begin{bmatrix} c_{B_1} & c_{B_2} \\ 0 & c_{B_4} \end{bmatrix} \times \begin{Bmatrix} \dot{B}_m \\ \dot{\tilde{B}}_m \end{Bmatrix} + \begin{bmatrix} k_{B_1} & k_{B_2} \\ k_{B_3} & k_{B_4} \end{bmatrix} \times \begin{Bmatrix} B_m \\ \tilde{B}_m \end{Bmatrix} = \begin{Bmatrix} f_{B_1} \\ f_{B_2} \end{Bmatrix} \tag{30}$$

In practice, the first space mode is determined to satisfy the initial condition on $\mathbf{T}$ and the final condition on $\boldsymbol{\lambda}$, then each mode m is determined based on the $m-1$ modes.

The second forward/backward problem

We follow the same procedure to solve the second coupled forward-backward problem (fourth equation in (19)). We introduce the separated form of the fields $\boldsymbol{\Lambda}$ and $\boldsymbol{\gamma}$, expressed in (31). In the same way as for the previous problem, we express the fields $\boldsymbol{\Lambda}_m$ and $\boldsymbol{\gamma}_m$ according to the space and the time variables, respectively through the functions $\mathbf{H}$ and $\tilde{\mathbf{H}}$, $K(t)$ and $\tilde{K}(t)$. We introduce the test fields $\delta\boldsymbol{\Lambda}_m$ and $\delta\boldsymbol{\gamma}_m$ (32) then we obtain a system whose solution leads to compute the space modes $\mathbf{H}$ and $\tilde{\mathbf{H}}$ and the time modes $K(t)$ and $\tilde{K}(t)$ by solving (33) and (34).

$$\begin{cases} \boldsymbol{\Lambda}_m = \sum_{n=1}^{m} \mathbf{H}_n \times K_n(t) \\ \boldsymbol{\gamma}_m = \sum_{n=1}^{m} \tilde{\mathbf{H}}_n \times \tilde{K}_n(t) \end{cases} \tag{31}$$

$$\begin{cases} \delta\boldsymbol{\Lambda}_m = \delta\mathbf{H}_m K_m(t) + \mathbf{H}_m \delta K_m(t) \\ \delta\boldsymbol{\gamma}_m = \delta\tilde{\mathbf{H}}_m \tilde{K}_m(t) + \tilde{\mathbf{H}}_m \delta\tilde{K}_m(t) \end{cases} \tag{32}$$

$$\begin{vmatrix} k_{H_1} & k_{H_2} \\ k_{H_3} & k_{H_4} \end{vmatrix} \times \begin{Bmatrix} \mathbf{H}_m \\ \tilde{\mathbf{H}}_m \end{Bmatrix} = \begin{Bmatrix} f_{H_1} \\ f_{H_2} \end{Bmatrix} \tag{33}$$

$$\begin{bmatrix} c_{K_1} & c_{K_2} \\ 0 & c_{K_4} \end{bmatrix} \times \begin{Bmatrix} \dot{K}_m \\ \dot{\tilde{K}}_m \end{Bmatrix} + \begin{bmatrix} k_{K_1} & k_{K_2} \\ k_{K_3} & k_{K_4} \end{bmatrix} \times \begin{Bmatrix} K_m \\ \tilde{K}_m \end{Bmatrix} = \begin{Bmatrix} f_{K_1} \\ f_{K_2} \end{Bmatrix} \tag{34}$$

The procedure is detailed in the Appendix where all the parameters of Eqs. (29), (30), (33) and (34) are explicitly expressed. The Appendix is in the Electronic Supplementary Material (ESM) of the online version of this paper.

Let us notice that the *PGD* method leads to solve the coupled forward-backward problems (third and fourth equations in (19)) as two separated problems each and this leads to drastically reduce the computation time.

6 Thermal building applications

6.1 Academic case study: 1D transient heat transfer through a building wall

To assess the goal-oriented inverse method performance on the prediction of a quantity of interest and on the identification of the model parameters involved in its computation, we apply the method on a 1D transient heat transfer problem through a building wall (*cf* Fig. 2). This problem corresponds to the one described by the mono-zone model (see Fig. 1) where the heat exchange at the internal wall surface is an imposed heat flux $q_0(t)$ and the heat exchange at the external wall surface is considered null. This simplification is done in order to obtain a problem whose analytical solution is known. The benefit of the analytical solution is to help understanding, explaining and validating the numerical results of the proposed goal-oriented inverse technique. It is also used to get the analytical expression, depending on the model parameters, of the studied quantities of interest. These analytical expressions are considered as reference thereafter to show that the goal-oriented inverse method properly selects and updates the model parameters that have the greatest influence on the quantity of interest.

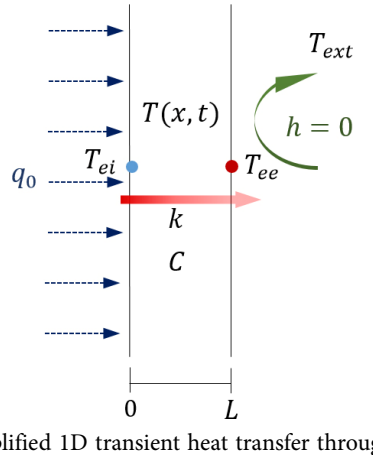

Fig. 2 A simplified 1D transient heat transfer through a building wall

When considering an imposed heat flux $q_0(t)$ with a ramp evolution in time, we can show that the analytical solution is

$$\begin{aligned} T(x,t) = T_0(x) + \frac{\delta q_0 t^2}{2cL} + \frac{\delta q_0 t}{6Lk}\left(3(x-L)^2 - L^2\right) \\ + \sum_{n=1}^{\infty} \frac{2cL^3\delta q_0}{n^4\pi^4 k^2} \cos\left(\frac{n\pi x}{L}\right)\left(\exp\left(-\frac{n^2\pi^2 kt}{cL^2}\right) - 1\right) \end{aligned} \tag{35}$$

where $T_0(x)$ is the initial temperature in the wall of thickness L and δq_0 is the slope of the ramp in W/(m²·s) such that $q_0 = \delta q_0 t$.

The studied problem has two unknown parameters, *i.e.* two potential parameters to be identified: the wall global heat conduction coefficient k and its global heat capacity c. We consider two temperature sensors: T_{ei} at the inside wall surface and T_{ee} at the outside wall surface. The measurement data are numerically generated using the direct heat transfer model (3) with the exact set of parameters:

$$\begin{aligned} &k_{ex} = 2\ \text{W/(K}\cdot\text{m)}, \quad c_{ex} = 2.2\times10^6\ \text{J/(K}\cdot\text{m}^3\text{)} \\ &L = 0.2\ \text{m}, \quad T_0(x) = 8\ ^\circ\text{C}, \quad \delta q_0 = 1.157\times10^{-2}\ \text{W/(m}^2\cdot\text{s)} \end{aligned} \tag{36}$$

which corresponds to a category of concrete building walls. A white noise $\mathcal{N}(0,\sigma)$ with $\sigma = 0.5$ °C is added to the synthetic sensor outputs.

In the inverse modeling strategy, we take as initial guess the parameters:

$$k_0 = 0.6k_{ex}, \quad c_0 = 0.6c_{ex} \tag{37}$$

As presented in Section 4, the proposed goal-oriented inverse method involves two specific parameters. The parameter τ being a characteristic time, it is chosen as $\tau = (c_0 / k_0) \times L^2$. Concerning the regularization parameter α, it is selected according to Morozov's principle (Morozov 1966) such that the data misfit at the end of the model updating process is slightly higher than the measurement error. For the verification of the Morozov principle in the goal-oriented inverse method, the considered data misfit is the gap between the temperature sensor outputs and the temperature field T_2, which is the extrapolation of the measurements with the numerical model computed from Eq. (13). In the following, the inverse method is illustrated on two quantities of interest. In both cases, the exact value of the quantity of interest is computed using the exact temperature $T_{ex}(x, t)$ obtained from the thermal building model with the exact set of parameters k_{ex} and c_{ex}, which would be unknown in practice.

6.2 First quantity of interest

The first studied quantity of interest is

$$Q^A = \frac{1}{L(t_2 - t_1)} \int_{t_1}^{t_2} (T(x=0,t) - T(x=L,t)) \mathrm{d}t \qquad (38)$$

Let us notice that the quantity $k \times Q^A$ corresponds to the averaged heat flux transferred through the wall between times t_1 and t_2. Herein, t_1 = 8 h and t_2 = 10 h. From the analytical solution (35), we can show that the quantity of interest Q^A is much more sensitive to the wall global heat conduction coefficient k than to the global heat capacity c. Hence, a robust prediction of the quantity of interest should be achieved by only updating the parameter k.

In Fig. 3, we present the results at the initial stage and at the end of the goal-oriented model updating process. The regularization parameter was set to α = 500 to satisfy the Morozov principle. At the initial stage, the error on the model parameters k and c is around 40% leading to an error of about 67% on the quantity of interest Q^A. When applying the goal-oriented inverse method, as expected we can see that only the parameter k is updated and the error on this parameter is drastically reduced to 3%. The quantity of interest Q^A being mostly sensitive to the parameter k, the proper identification of this parameter conducts to a robust estimation of the quantity of interest. The time evolution of the temperature sensor outputs and the predicted temperatures T_1 and T_2, before and after the goal-oriented model updating process, are compared in Fig. 4. We recall that T_1 is computed from a finite element direct solution of the building thermal equations and T_2 is a temperature field coupling sensor outputs and the physical model via the weight parameter α. This parameter being selected to 500, which gives an important weight to the sensor outputs, we can see that the temperature T_2 is closer to the measured temperature than the numerical temperature T_1 derived from the physical model. In Fig. 4, the quantity of interest Q^A is represented in a graphical way. In this particular case, let us notice that Q^A can be fully computed from the sensor outputs. The goal is to graphically compare the predicted quantity of interest derived form the inverse method and the exact quantity of interest. In Fig. 4 the exact quantity of interest, ignoring the multiplication scalar factor $1/(L(t_2 - t_1))$, corresponds to the red dashed-lines hatched area whereas the predicted quantity of interest is represented by the yellow colored area. At the initial stage (Fig. 4), it can be noticed that the quantity of interest is overestimated, *i.e.* the yellow-colored area is larger than the area in red dashed lines. Once the goal-oriented inverse method has correctly identified the parameter k, we can see that both areas (bottom of Fig. 4) are approximately the same. Although the error between the calculated and the measured values of the quantity of interest is small, the gap between the temperature T_1 predicted from the physical model and the temperature sensor outputs remains relatively large. Indeed, the considered

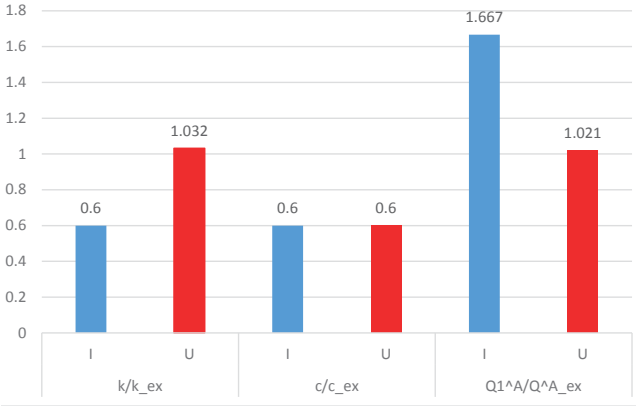

Fig. 3 Numerical results at the initial stage, denoted "I", and at the end of the goal-oriented model updating process, denoted "U", considering the quantity of interest Q^A ($Q^A_{ex} = 83.3$ K/m)

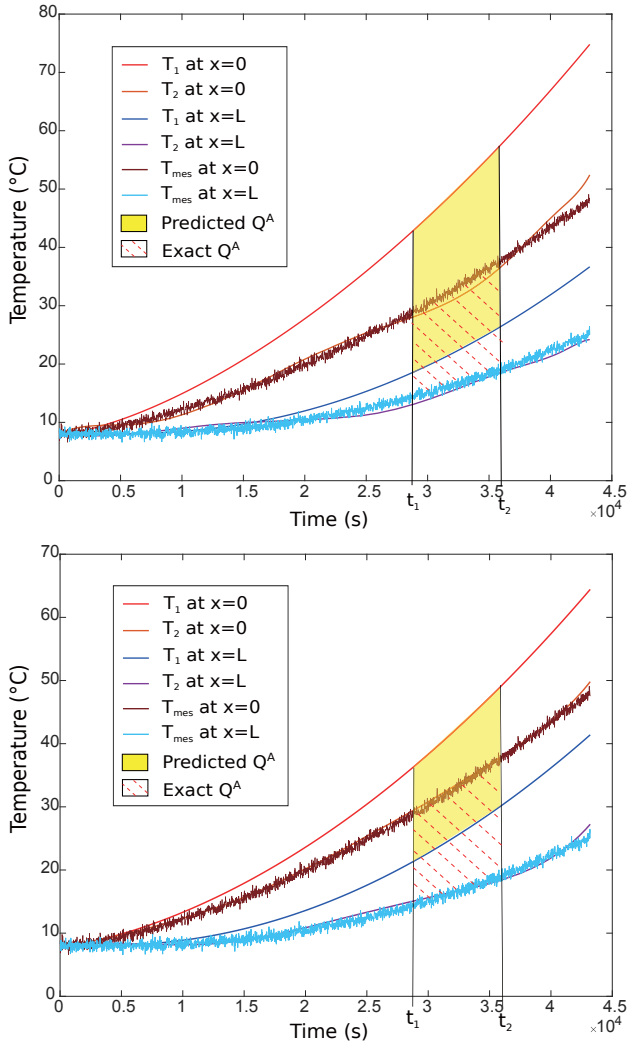

Fig. 4 Comparison of temperature sensor outputs and predicted temperature at the initial stage (top) and after the goal-oriented model updating process (bottom). The predicted (resp. exact) quantity of interest Q^A, ignoring the multiplication scalar factor $1/(L(t_2 - t_1))$, is represented by yellow-colored area (resp. using red dashed-lines area)

quantity of interest Q^A allows an accurate prediction of the temperature difference, while the absolute temperature is not accurate, such as infrared temperature measurement. To summarize, even if the predicted temperatures do not fit the temperature sensor outputs like in standard inverse techniques, the objective of a reliable prediction of the quantity of interest is reached.

6.3 Second quantity of interest

Let us now consider the quantity of interest defined as

$$Q^B = \int_0^L (T(x, t = t_2) - T(x, t = t_1))\mathrm{d}x \quad (39)$$

It can be noticed that $c \times Q^B$ corresponds to the stored energy in the wall over the time interval $[t_1, t_2]$. As previously, t_1 = 8 h and t_2 = 10 h. In this case, it can be shown from the analytical solution that the global heat capacity c has a significant influence on Q^B contrary to the wall global heat conduction coefficient k.

To ensure Morozov's discrepancy principle, the numerical value of the regularization parameter is determined to α = 200. The results at the initial stage and at the end of the model updating process are summarized in Fig. 5. The parameter c, having a major impact on the quantity of interest, is suitably estimated with an error below 10% while the parameter k is not updated. Hence, the error on the prediction of the quantity of interest goes from 67% at the initial stage to 8% after the goal-oriented inverse process. The definition of the quantity of interest Q^B involves the temperature gap $T(x, t_2) - T(x, t_1)$. In Fig. 6, we compare the temperature gap obtained in different ways, notably using:

- the temperature T_1, defined in Section 4, at the initial stage and at the end of the goal-oriented process;
- the temperature T_2, defined in Section 4, at the initial stage and at the end of the goal-oriented process;
- the exact temperature field, computed with the direct physical model and the exact set of parameter k_{ex} and c_{ex}, which would be unknown in practice.

From this temperature gap, we represent the exact quantity of interest using the red dashed-lines hatched area and the predicted quantity of interest, at the initial and the final stage of the inverse technique, using a yellow-colored area. In the lower graph in Fig. 6, we note that at the end of the goal-oriented inverse process the spatial temperature curves have intersection points, which means that the error between the calculated temperature difference and the measured temperature difference is not always reduced. Contrary to standard inverse techniques, the calculated temperature has not to fit the sensor outputs point by point but only to accurately predict the quantity of interest, which

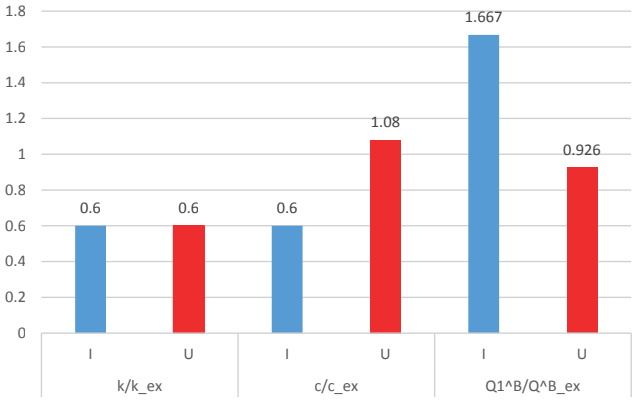

Fig. 5 Numerical results at the initial stage, denoted "I", and at the end of the goal-oriented model updating process, denoted "U", considering the quantity of interest Q^B ($Q^B_{ex} = 1.228\ \mathrm{K \cdot m}$).

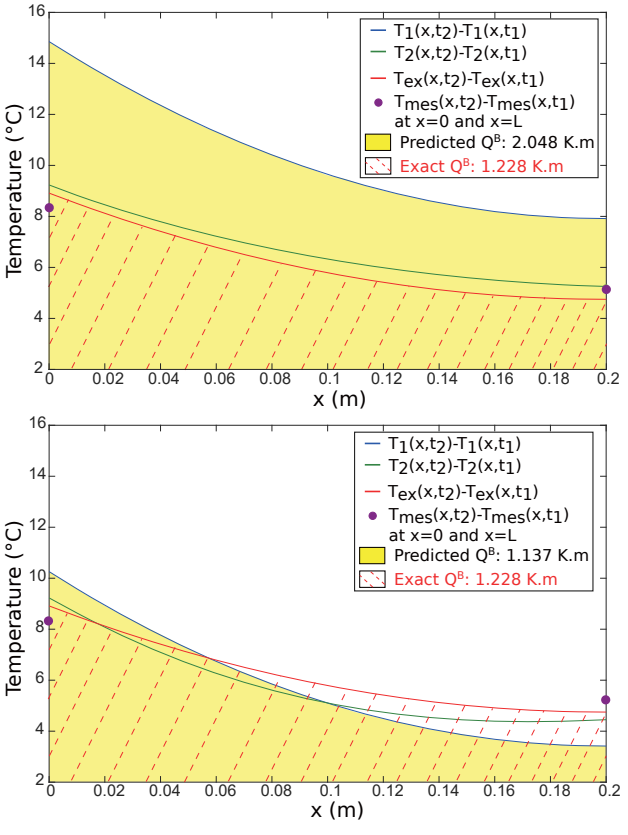

Fig. 6 Comparison of temperature gap between time t_1, and t_2, involved in the quantity of interest Q^B , at the initial stage (top) and after the goal-oriented model updating process (bottom). The sensor outputs at the internal and the external faces of the wall are indicated by a circle. The predicted quantity of interest Q^B is represented in yellow color - The exact quantity of interest Q^B , depicted by the red dashed-line area, is computed using the exact temperature gap $T_{ex}(x, t_2) - T_{ex}(x, t_1)$ obtained from the building thermal model with the exact set of parameters k_{ex} and c_{ex}

corresponds herein to an integral on the whole envelope. Graphically, the yellow area has to fit the red dashed-lines hatched area. At the initial stage, we observe that the predicted

quantity of interest Q^B, *i.e.* 2.048 K·m, is overestimated by about 67%. Nevertheless, at the end of the goal-oriented inverse process we can see that the predicted quantity of interest Q^B, *i.e.* 1.137 K·m, draws with the exact quantity of interest, *i.e.* 1.228 K·m, but due to measurement error it is underestimated by about 8% as mentioned in Fig. 5.

Lastly, we compare the results of the standard Tikhonov regularization inverse method and of the proposed goal-oriented inverse method. In both methods, the updating process stops when the modification of the parameters is less than 0.5%. Contrary to the goal-oriented technique, the Tikhonov approach updates all the model parameters, *i.e, c* and *k*, in view of minimizing the data misfit functional. Hence, the Tikhonov method better reproduces the temperature sensor outputs. The quantities of interest Q^A and Q^B computed at each iteration of Tikhonov and goal-oriented methods are summarized in Table 1. Results show that the goal-oriented inverse method stops after 4 iterations and that the updated quantities of interest converge faster to the exact value of the quantity of interest for the goal-oriented method than the inverse Tikhonov technique.

Table 1 Computations of quantities of interest Q^A and Q^B at each iteration of the standard inverse method with Tikhonov regularization and of the goal-oriented inverse technique

Iteration number	Tikhonov Q^A/Q^A_{ex}	Goal-oriented Q^A/Q^A_{ex}	Tikhonov Q^B/Q^B_{ex}	Goal-oriented Q^B/Q^B_{ex}
1	1.668	1.668	1.668	1.668
2	1.358	1.159	1.147	1.111
3	1.073	1.033	0.907	0.980
4	1.070	1.022	0.958	0.926
5	1.019	—	0.976	—
6	1.014	—	0.985	—
7	1.009	—	0.982	—
8	1.007	—	0.987	—

To conclude, we showed in the academic study case that the goal-oriented inverse method targets and properly updates the model parameter in view of improving the prediction of the quantity of interest. Although the goal-oriented inverse method does not precisely reproduce the temperature sensor outputs as the Tikhonov method, the proposed inverse method can be more relevant to get an accurate prediction of a quantity of interest. To demonstrate the abilities of the proposed inverse technique for operational applications, it is applied to a real thermal building problem with real sensor outputs in the next section.

6.4 Real case: application to the "Sense-City" chalet

The second example deals with a mono-zone thermal model representing an experimental real-size wooden chalet that belongs to the equipment "Sense-City" (Derkx et al. 2012) located in Marne-la-Vallée, France (left of Fig. 7). The studied chalet is 20 m^2 area and 2.7 m height. Its envelope is made of a wood layer of 44 mm thickness and is provided with an interior insulation layer (polystyrene) of 60 mm thickness and a plaster layer of 10 mm thickness. Due to air quality experiments in this chalet, the mechanical ventilation system was designed at 100 m^3/h.

In this application, we choose to model the chalet using a resistor-capacitance network based on the analogy between the heat transfer and the electric current flow. In such models the building envelope is modeled by a set of resistors and capacitors while the thermal zone is modeled by only a capacitor (Deng et al. 2010; Goyal and Barooah 2011). These models are used in several studies to describe the building thermal behavior at a low computational cost especially in optimal control applications such as in (Bartaud du Chazaud and Baleynaud 2016; Berthou et al. 2013). In the present work, the building is described by a 6R2C model, *i.e.* using six resistors and two capacitors. The 6R2C model

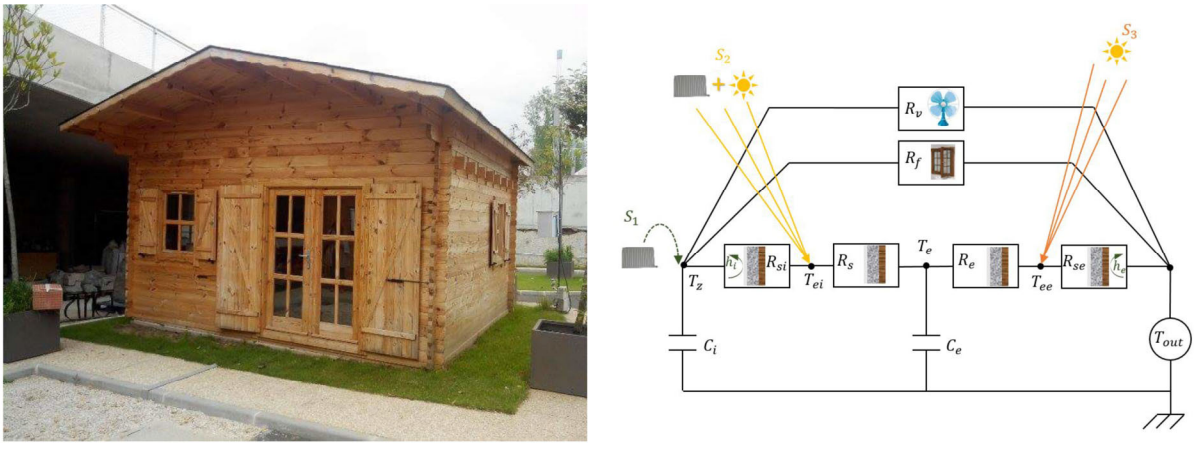

Fig. 7 The studied building (left) and its associated 6R2C thermal model (right)

is a simple model but detailed enough to take into account all the heat exchange modes and thedifferent heat loads, such as the solar and the internal gains. Many studies showed that despite its simplicity, this model predicts the building thermal behavior with an acceptable accuracy, see for instance (Berthou et al. 2013; Faggianelli et al. 2015). This model integrates three heat loads identified as S_1, S_2 and S_3,: S_1,, assigned to the node T_z, gathers the convective internal gains due to the heating system and the occupancy; S_2, applied on the node T_{ei}, contains the radiative internal gains due to the heating system, the occupancy and the solar gains arriving inside the thermal zone; and S_3, applied on the node T_{ee}, represents the incident solar gains on the outside envelope surface. In practice, as the chalet is unoccupied S_1 includes only the heating systems. The chalet having small window area, the solar gains arriving inside the thermal zone are not considered. The gain S_2 is taken equal to zero (no occupancy, no radiative part due to the heating system and no solar gain). Concerning the solar radiation, we can see from the meteorological station data given in the supplementary material that its direct component is negligible with respect to its diffuse part. It is an expected observation for a thermal study in December in the north of France. We also suppose the reflected solar radiation is negligible. Hence, the absorbed incident solar gains S_3 on the outside envelope surface, involved in the RC model, is computed herein by:

$$S_3 = 0.5 \times A \times \alpha_e \times \phi_{diff} \tag{40}$$

where ϕ_{diff} corresponds to the diffuse solar radiation in W/m^2 measured on an horizontal panel by the meteorological station (see supplementary material data), α_e is the absorption rate taken to 0.6, A = 40.2 m^2 is the surface of the outside envelope and the standard coefficient 0.5 is associated to the fact that the solar radiation hits vertical faces.

Then, the RC model equations are obtained by writing the thermal balance at the nodes T_z, T_{ei}, T_e and T_{ee} where these nodes represent respectively the inside thermal zone temperature, the inside envelope surface temperature, the envelope temperature and the outside envelope surface temperature. For convenience, the model Eq. (41) are written using the thermal transmittance parameter U, *i.e.* the inverse of the resistance R, in a compacted matrix form. One can notice that this problem has the same structure as the direct heat transfer problem described in Section 4, that means that the goal-oriented inverse method can be easily applied on this problem without significant changes in its formulation.

$$\mathbb{C}\dot{\mathbf{T}} + \mathbb{K}\mathbf{T} = \mathbf{F} \tag{41}$$

with

$$\mathbb{C} = \begin{bmatrix} C_z & 0 & 0 & 0 \\ 0 & 0 & 0 & 0 \\ 0 & 0 & C_e & 0 \\ 0 & 0 & 0 & 0 \end{bmatrix},$$

$$\mathbb{K} = \begin{bmatrix} (U_{si} + U_v + U_f) & -U_{si} & 0 & 0 \\ -U_{si} & (U_{si} + U_s) & -U_s & 0 \\ 0 & -U_s & (U_s + U_e) & -U_e \\ 0 & 0 & -U_e & (U_e + U_{se}) \end{bmatrix} \tag{42}$$

and

$$\mathbf{F} = \begin{Bmatrix} S_1 + (U_v + U_f)\mathbf{T}_{out} \\ S_2 \\ 0 \\ S_3 + U_{ee}\mathbf{T}_{out} \end{Bmatrix},$$

$$\mathbf{T} = \begin{Bmatrix} T_z \\ T_{ei} \\ T_e \\ T_{ee} \end{Bmatrix} \tag{43}$$

The thermal behavior of the chalet was studied on a period of 38 hours in February 2018. The chalet was submitted alternately to 1600 W heating and free cooling periods. The ventilation was operating at 100 m^3/h during the whole studied time period. Concerning the sensors, the chalet was equipped with PT100 temperature sensors in the room, denoted T_z^{mes}, on the inside and the outside faces of the north oriented wall, denoted T_{ei}^{mes} and T_{ee}^{mes}. Two flux sensors with the dimensions 300 mm × 300 mm were also placed on the inside and the outside faces of the north-oriented wall. Lastly, a local weather station was deployed to get the outside temperature, denoted T_{out}, and the diffusive and the direct solar fluxes. All the sensors outputs data are available in the Electronic Supplementary Material (ESM) of the online version of this paper.

From the technical characteristics of the chalet, we propose in Table 2 an initial set of model parameters. Using this initial set of parameters, the thermal behavior of the chalet is simulated and compared to the sensor outputs in Fig. 8. Although the predicted temperatures (without model updating process) are underestimated, we can see that the predicted flux on the inside wall surface is close to the measured one (less than 10% discrepancy). Nevertheless, we observe a different trend between the measured and the calculated heat fluxes at the interior wall surface, notably during the period 18 h–24 h. On the one hand, when the heating is switched on at t = 18 h, the measured zone temperature T_z^{mes} increases much faster than the measured temperature at the inside wall face T_{ei}^{mes} which leads to the

Table 2 Initial set of the parameters of the 6R2C model

U_{si}^0 (W/K)	U_s^0 (W/K)	U_e^0 (W/K)	U_{se}^0 (W/K)	U_f^0 (W/K)	U_v^0 (W/K)	C_i^0 (J/K)	C_m^0 (J/K)
200	200	35	1140	14	32	7.33×10^5	1.60×10^6

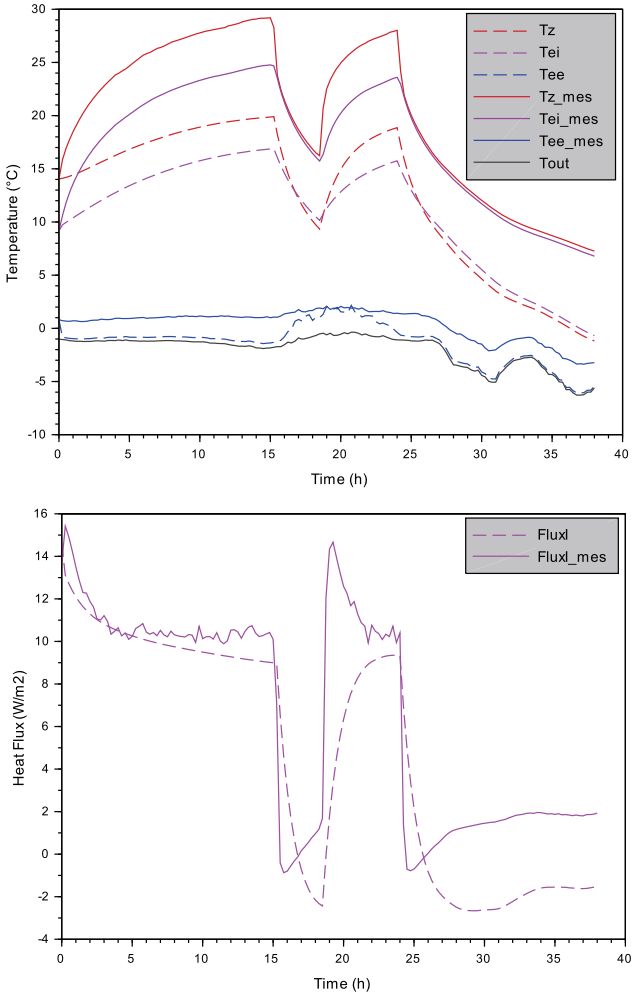

Fig. 8 Simulated and measured temperatures (top), simulated and measured heat flux at the interior wall surface (bottom). Simulation using 6R2C model with initial set of parameters defined in Table 2. Solid lines (resp. dashed lines) correspond to measurement (resp. simulation)

peak at t = 19 h of the measured flux on the inside wall face. Then, the measured gap between the zone and the inside wall face temperatures reduces between t = 19 h and t = 24 h and thus the measured flux decreases. On the other hand, we see in Fig. 8 that the calculated flux on the inside wall face grows steadily from t = 18 h to t = 24 h. It may be explained by an overestimation of the zone thermal capacitance value C_i^0 implying a low rise of the simulated zone temperature and a steadily grow of the gap between the zone and the inside face numerical temperatures. Moreover, we can see in Fig. 8 that the increase of the simulated outside surface temperature between t = 16 h and t = 25 h (due to solar radiation) is higher than the measured one. It may be due to the fact that the studied chalet is located close to a large building and thus a part of the solar radiation could have been masked. As we don't consider shading effects in the expression of the solar gain S_3, the estimated solar radiation may be overestimated which leads to a significant temperature increase.

The flow rate of the ventilation system was measured using a 1D hot wire anemometer and was found in agreement with the manufacturer data. Hence, the ventilation thermal transmittance U_v is considered well-controlled and it is not updated in the followings. To proceed, we apply inverse modeling techniques in the next paragraphs to update the 7 parameters U_{si}, U_s, U_e, U_{se}, U_f, C_i, C_m involved in the 6R2C thermal building model using the measured temperatures T_z, T_{ei} and T_{ee}. Two inverse methods are compared: a classical data misfit approach with Tikhonov regularization and the proposed goal-oriented inverse method. In both inverse methods, the regularization parameter is chosen to ensure an extended discrepancy principle taking into account the measurement and the model errors. It consists in choosing the regularization parameter such that the data misfit at the end of the inverse processes is close and strictly higher than a threshold J_S defined below involving the model and the measurement errors. We recall that the considered data misfit in the goal-oriented inverse method is the gap between the temperature sensor outputs and the temperature field T_2, which is the extrapolation of the measurements with the numerical model computed from Eq. (13). In the experiment, only PT100 probes were deployed to monitor the temperatures. The measurement error ϵ^{mes} of the PT100 temperature sensors and the acquisition system were evaluated to 0.5 °C by the metrology department at IFSTTAR. Concerning the model error ϵ^{mod}, for simplicity it was empirically estimated to 1 °C. For a better evaluation of the model error, *a posteriori* model error estimators can be used (Braack and Ern 2003; Li et al. 2015; Oden and Prudhomme 2002). From these errors, we define a data misfit threshold

$$J_S = \sum_{n=1}^{n_s} \frac{1}{2} \int_{t=0}^{t=t_f} (\epsilon^{mes} + \epsilon^{mod})^2 \, dt = 4.6\times10^5 \ s\cdot K^2 \qquad (44)$$

where n_s = 3 is the number of temperature sensors.

To apply the goal-oriented inverse method detailed in Section 4, one also needs to fix an additional parameter that is a building characteristic time τ in seconds. Herein, we take τ = 374 min ≈ 6 h .

Definition of quantities of interest

In the following, we again focus on two quantities of interest Q^C and Q^D defined as

$$\begin{cases} Q^C = \int_{t=8\text{h}}^{t=12\text{h}} U_{\text{si}}(T_{\text{z}} - T_{\text{ei}})\text{d}t \\ Q^D = \dfrac{1}{t_2 - t_1}\int_{t_1=14\text{h}}^{t_2=15\text{h}} T_{\text{z}}\text{d}t \end{cases} \quad (45)$$

On the one hand, the quantity of interest Q^C is related to the interior heat flux between the room and the inside wall face during a heating period. It is highly dependent on the indoor exchange coefficient h_{i} involved in the thermal transmittance U_{si}. Let us remark that Q^C is an energy. On the other hand, the quantity of interest Q^D corresponds to the mean value of the room temperature during one hour at the end of the first heating period. To evaluate the quality of the prediction on the quantities of interest by the different inverse techniques, they are measured using heat flux and temperature sensors respectively.

Model updating with a standard Tikhonov approach

In the standard inverse approach, 27 iterations are performed to determine the updated parameters. At each iteration, one has to perform:

- the solution of the direct 6R2C Eq. (41)
- the solution of the adjoint 6R2C equations to get the gradient direction
- several solutions of the direct 6R2C equations to find the optimal descent step.

As previously, the model updating process stops when the modification on the parameters are less than 0.5%. The numerical values of the updated model parameters at the end of the inverse modeling process are summarized in Table 3. As expected, all the parameters are adjusted using Tikhonov's approach except the ventilation thermal transmittance U_{v} considered well-mastered. We can notice that the parameters associated to air infiltration and the envelope are the most corrected, *i.e.* the air infiltration thermal transmittance U_{f} (resp. the envelope thermal transmittance U_{e}) is reduced by about 87% (resp. 70%). After updating the model parameters, the simulated temperatures better approximate the measured temperatures (see Fig. 9) except for the outside surface temperature. We observe that the fluctuations of the outside surface temperature within 15–25 hours due to solar gains are overestimated in the numerical simulation compared to the measurement. This may be due to a coarse estimation of the incident solar gains S_3 on the outside envelope surface from the diffusive and the direct fluxes measured by the weather station. To improve its estimation, the solar gain S_3 can be weighted by a multiplier coefficient which will be identified in the inverse problem. Lastly, the updated quantities of interest Q^C and Q^D at each iteration of the inverse procedure are given in Fig. 10. With the initial set of parameters, we observe that the gap between the predicted and the measured quantity of interest is less than 10% for Q^C and higher than 30% for Q^D. Indeed, we get a suitable approximation of the heat flux, as the temperature gap between the room and on the inside wall face is well predicted, while the room temperature T_{z} is coarsely determined. By minimizing the temperature data misfit in the inverse procedure, we see that the room temperature slowly converges to the measured room temperature. After 27 iterations, the error between the predicted and the measured quantity of interest Q^D is about 3%. Nevertheless, for the quantity of interest Q^C we remark that the prediction of the heat flux is deteriorated when using standard classical Tikhonov technique. This may be due to the fact that the minimization problem is formulated on temperatures and not on heat fluxes.

Table 3 Updates of 6R2C model parameters using different inverse techniques: data misfit minimization with Tikhonov regularization (Tikh.), goal-oriented inverse methods considering quantity of interest Q^C (G-O - Q^C) and quantity of interest Q^D (G-O - Q^D). U^{upd} denotes the updated model parameter at the end of the inverse processes

	$\frac{U_{\text{si}}^{\text{upd}}}{U_{\text{si}}^0}$	$\frac{U_{\text{s}}^{\text{upd}}}{U_{\text{s}}^0}$	$\frac{U_{\text{e}}^{\text{upd}}}{U_{\text{e}}^0}$	$\frac{U_{\text{se}}^{\text{upd}}}{U_{\text{se}}^0}$	$\frac{U_{\text{f}}^{\text{upd}}}{U_{\text{f}}^0}$	$\frac{U_{\text{v}}^{\text{upd}}}{U_{\text{v}}^0}$	$\frac{U_{\text{i}}^{\text{upd}}}{U_{\text{i}}^0}$	$\frac{U_{\text{m}}^{\text{upd}}}{U_{\text{m}}^0}$
Tikh.	0.895	0.404	0.307	0.861	0.134	1	0.840	1.308
G-O - Q^C	1	1	1	1	1	1	1	1
G-O - Q^D	1	1	1	1	0.145	1	1	1

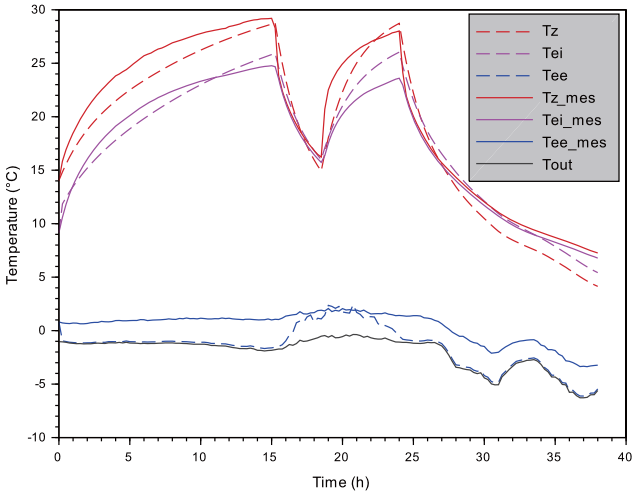

Fig. 9 Temperatures obtained at the end of the data misfit minimization with Tikhonov regularization and the measured temperatures. Solid lines (resp. dashed lines) correspond to measurement (resp. simulation)

Model updating with goal-oriented inverse method applied to quantity of interest Q^C

To satisfy the extended discrepancy principle taking into account both measurement and model errors, the regularization parameter α is set to 20. At the first iteration

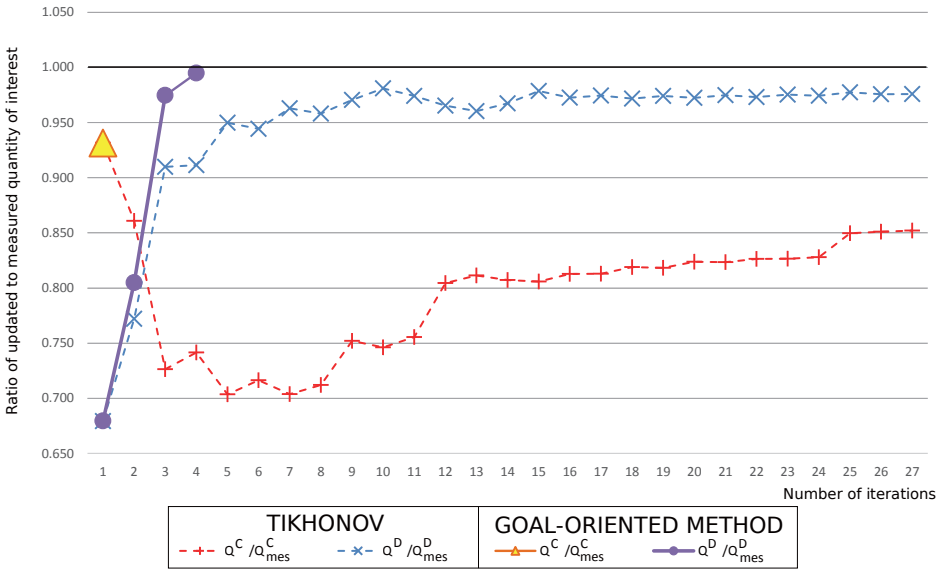

Fig. 10 Ratio of updated quantity of interest to measured quantity of interest at each iteration of Tikhonov and goal-oriented inverse techniques

of the goal-oriented inverse process, the highest component of the functional gradient is obtained for the thermal transmittance U_{si}, which is explicitly involved in the formula of Q^C. Hence, the parameter U_{si} is selected for an update. Nevertheless after testing various values of U_{si}, the goal-oriented functional does not decrease, which means that the quantity of interest Q^C is not improved, and leads to stop the inverse process. The goal-oriented inverse method detects that the quantity of interest Q^C is well predicted using the initial model parameters and preferred to stop at iteration 1 rather than deteriorating the prediction of Q^C. No parameter is updated as shown in Table 3.

Model updating with goal-oriented inverse method applied to quantity of interest Q^D

Herein, we take the regularization parameter $\alpha = 5$ to verify the extended discrepancy principle. In Fig. 10, we observe that the updated quantity of interest Q^D with the goal-oriented inverse method converges faster to the measured quantity of interest than the one updated with the classical Tikhonov method. After 3 iterations, the error on the quantity of interest Q^D is about 3% with the goal-oriented inverse method while it is about 10% for the classical Tikhonov method. The goal-oriented inverse method indicates that the model parameter U_f is the most sensitive parameter to improve the prediction on Q^D and thus it focuses on its correction. Consequently, in Table 3 we observe that only U_f is updated with the goal-oriented inverse method and that it stops at iteration 4. Let us notice that the updated values of the thermal transmittance U_f by Tikhonov and goal-oriented methods are similar, which is consistent.

To conclude, the goal-oriented inverse method has been applied to an academical study case where the analytical solution is known. In this case considered as a numerical proof, we verified that the proposed method properly updates only the model parameters having a significant impact on the quantity of interest. Then, we showed that the goal-oriented inverse method can be applied to a real building using a common resistor-capacitor model. In that cases, a robust prediction of the quantity of interest is obtained faster compared to a classical Tikhonov technique.

7 Conclusion and prospects

We proposed an inverse methodology combining the goal-oriented inverse method and the proper generalized decomposition to sharply predict a quantity of interest in thermal building problems. Unlike the standard inverse methods that aim at identifying all the model parameters in order to fit the data measurements, the goal-oriented inverse strategy focuses on the prediction of a quantity of interest and thus updates only the model parameters involved in its computation.

This assumption was verified through four examples of quantities of interest. We first applied the goal-oriented inverse method on a numerical problem, with synthetic data, whose analytical solution is known and we demonstrated through two examples of quantities of interest that the proposed method accurately identifies the quantity of interest by updating only the model parameter to which it is the most sensitive.

A second example was dedicated to a 6R2C real building model where the indoor temperature and the inner and outer surface temperatures of the north wall were measured. The results were compared to those obtained using the Tikhonov regularization method and showed that the goal-oriented method predicts the sought quantity of interest faster (less iterations) and more accurately than the Tikhonov method. Indeed, the Tikhonov method sometimes deteriorates the predicted quantity of interest when trying to fit the computed temperature to the measured one. In summary, Tikhonov's methods are more relevant to assess the global thermal behavior of a building but the goal-oriented inverse method should be rather selected for the prediction of a quantity of interest.

The goal-oriented inverse method may have other advantages that were not tackled in this paper. Indeed, thanks to its formulation, the goal-oriented inverse method may lead to reduce the number of sensors required to accurately predict the quantity of interest and its combination with the *PGD* method would lead to optimize their positions. The outlines of a sensor placement strategy derived from the goal-oriented approach was previously proposed in (Chamoin et al. 2014). In a future article, this goal-oriented sensor placement method will be addressed and applied to more complex real buildings, including several thermal zones and a larger number of parameters.

Acknowledgments

The authors acknowledge support from the project Sense-City funded by ANR (France) within the Investment for the Future Program under reference number ANR-10-EQPX-48. We would like to thank the Sense-City team, and particularly Erick Merliot for his technical advice and support during the sensors deployment.

Electronic Supplementary Material (ESM): supplementary material is available in the online version of this article at https://doi.org/10.1007/s12273-020-0603-8. ESM files include the Appendix and all the sensors outputs data.

References

Alekseev AK, Navon IM (2010). Criteria of optimality for sensors' location based on adjoint transformation of observation data interpolation error. *International Journal for Numerical Methods in Fluids*, 62: 74–89.

Allix O, Ladevèze P, Gilletta D, Ohayon R (1989). A damage prediction method for composite structures. *International Journal for Numerical Methods in Engineering*, 27: 271–283.

Allix O, Feissel P, Nguyen HM (2005). Identification strategy in the presence of corrupted measurements. *Engineering Computations*, 22: 487–504.

Alzetto F, Pandraud G, Fitton R, Heusler I, Sinnesbichler H (2018). QUB: A fast dynamic method for *in situ* measurement of the whole building heat loss. *Energy and Buildings*, 174: 124–133.

Artiges N (2016). De l'instrumentation au contrôle optimal prédictif pour la performance énergétique du bâtiment. PhD Thesis, Université Grenoble Alpes, France. (in French)

Bartaud du Chazaud E, Baleynaud J (2016). Contribution à la mise au point d'un modèle "en boite grise" pour le contrôle prédictif de la consommation énergétique des bâtiments. In: Congrès de la Société Francaise de thermique.

Becker R, Vexler B (2004). A posteriori error estimation for finite element discretization of parameter identification problems. *Numerische Mathematik*, 96: 435–459.

Berger J, Gasparin S, Chhay M, Mendes N (2016a). Estimation of temperature-dependent thermal conductivity using proper generalised decomposition for building energy management. *Journal of Building Physics*, 40: 235–262.

Berger J, Orlande HRB, Mendes N, Guernouti S (2016b). Bayesian inference for estimating thermal properties of a historic building wall. *Building and Environment*, 106: 327–339.

Berger J, Mendes N, Guernouti S, Woloszyn M, Chinesta F (2017a). Review of reduced order models for heat and moisture transfer in building physics with emphasis in PGD approaches. *Archives of Computational Methods in Engineering*, 24: 655–667.

Berger J, Orlande HRB, Mendes N (2017b). Proper Generalized Decomposition model reduction in the Bayesian framework for solving inverse heat transfer problems. *Inverse Problems in Science and Engineering*, 25: 260–278.

Beringhier M, Gigliotti M (2015). A novel methodology for the rapid identification of the water diffusion coefficients of composite materials. *Composites Part A: Applied Science and Manufacturing*, 68: 212–218.

Berthou T, Stabat P, Salvazet R, Marchio D (2013). Optimal control for building heating: An elementary school case study. In: Proceedings of the 13th International IBPSA Building Simulation Conference, Chambéry, France.

Binev P, Cohen A, Mula O, Nichols J (2018). Greedy algorithms for optimal measurements selection in state estimation using reduced models. *ASA Journal on Uncertainty Quantification*, 6: 1101–1126.

Boisson P, Bouchié R (2014). ISABELE method: In-Situ Assesslent of the Building EnveLope pErformances. In: Proceedings of the 9th International Conference on System Simulation in Buildings, Liege, Belgium.

Bonnet M, Aquino W (2014). Three-dimensional transient elastodynamic inversion using the modified error in constitutive relation. *Journal of Physics: Conference Series*, 542: 012003.

Bouchié R, Alzetto F, Brun A, Boisson P, Thebaut S (2014). Short methodologies for in-situ assessment of the intrinsic thermal performance of the building envelope. In: Proceedings of Sustainable Places, Nice, France.

Bouclier R, Louf F, Chamoin L (2013). Real-time validation of mechanical models coupling PGD and constitutive relation error. *Computational Mechanics*, 52: 861–883.

Braack M, Ern A (2003). A posteriori control of modeling errors and discretization errors. *Multiscale Modeling & Simulation*, 1: 221–238.

Brouns J, Nassiopoulos A, Bourquin F, Limam K (2016). Dynamic building performance assessment using calibrated simulation. *Energy and Buildings*, 122: 160–174.

Bui HD, Constanctinescu A (2000). Spatial localization of the error of constitutive law for the identification of defects in elastic bodies. *Archives of Mechanics*, 52(4–5): 511–522.

Chamoin L, Ladevèze P, Waeytens J (2014). Goal-oriented updating of mechanical models using the adjoint framework. *Computational Mechanics*, 54: 1415–1430.

Chatterjee A (2000). An introduction to the proper orthogonal decomposition. Current Science, 78(7):10.

Chavent G, Kunisch K, Roberts J (1996). Primal-dual formulations for parameter identification problems. Research report, INRIA Research Report RR-2891.

Chinesta F, Ladeveze P, Cueto E (2011). A short review on model order reduction based on proper generalized decomposition. *Archives of Computational Methods in Engineering*, 18: 395–404.

Chinesta F, Keunings R, Leygue A (2014). The Proper Generalized Decomposition For Advanced Numerical Simulations. Cham, Switzerland: Springer.

Chinesta F, Huerta A, Rozza G, Willcox K (2017). Model order reduction. In: Stein E, Borst R, Hughes JTR (eds), Encyclopedia of Computational Mechanics, 2nd edn. Chichester, UK: John Wiley & Sons.

Chouaki A, Ladevèze P, Proslier L (1996). An updating of structural dynamic model with damping. In: Proceedings of the 2nd International Conference on Inverse Problems in Engineering: Theory and Practice, Le Croisic, France, pp. 335–342.

Daescu DN, Carmichael GR (2003). An adjoint sensitivity method for the adaptive location of the observations in air quality modeling. *Journal of the Atmospheric Sciences*, 60: 434–450.

De Simon L, Iglesias M, Jones B, Wood C (2018). Quantifying uncertainty in thermophysical properties of walls by means of Bayesian inversion. *Energy and Buildings*, 177: 220–245.

Deng K, Barooah P, Mehta PG, Meyn SP (2010). Building thermal model reduction via aggregation of states. In: Proceedings of American Control Conference, Baltimore, MD, USA.

Deraemaeker A, Ladevèze P, Leconte P (2002). Reduced bases for model updating in structural dynamics based on constitutive relation error. *Computer Methods in Applied Mechanics and Engineering*, 191: 2427–2444.

Derkx F, Lebental B, Bourouina T, Bourquin F, Cojocaru C-S, Robine E, Van Damme H (2012). The Sense-City project. In: Proceedings of XVIIIth Symposium on Vibrations, Shocks and Noise.

Faggianelli GA, Brun A, Wurtz E, Muselli M (2015). Grey-box modelling for naturally ventilated buildings. In: Proceedings of the 14th International IBPSA Building Simulation Conference, Hyderabad, India.

Feissel P, Allix O (2007). Modified constitutive relation error identification strategy for transient dynamics with corrupted data: The elastic case. *Computer Methods in Applied Mechanics and Engineering*, 196: 1968–1983.

Gagnon R, Gosselin L, Decker S (2018). Sensitivity analysis of energy performance and thermal comfort throughout building design process. *Energy and Buildings*, 164: 278–294.

Golub GH, Reinsch C (1970). Singular value decomposition and least squares solutions. *Numerische Mathematik*, 14: 403–420.

González D, Masson F, Poulhaon F, Leygue A, Cueto E, Chinesta F (2012). Proper Generalized Decomposition based dynamic data driven inverse identification. *Mathematics and Computers in Simulation*, 82: 1677–1695.

Goyal S, Barooah P (2011). A method for model-reduction of nonlinear building thermal dynamics. In: Proceedings of American Control Conference, San Francisco, CA, USA.

Hadamard J (1923). Lecture on Cauchy's Problem in Linear Partial Differential Equations. New Haven, CT, USA: Yale University Press.

Heiselberg P, Brohus H, Hesselholt A, Rasmussen HES, Seinre E, Thomas S (2007). Application of sensitivity analysis in design of sustainable buildings. In: Proceedings of Sustainable Development of Building and Environment (SDBE), Chongqing, China.

Hong T, Jiang Y (1997). A new multizone model for the simulation of building thermal performance. *Building and Environment*, 32: 123–128.

IEA (2019). Energy efficiency: Buildings. International Energy Agency. Available at https://www.iea.org/topics/energyefficiency/buildings/. Accessed 18 Sept 2019.

Johansson H, Runesson K, Larsson F (2007). Parameter identification with sensitivity assessment and error computation. *GAMM-Mitteilungen*, 30: 430–457.

Johansson H, Larsson F, Runesson K (2011). Application-specific error control for parameter identification problems. *International Journal for Numerical Methods in Biomedical Engineering*, 27: 608–618.

Kleiber M, Antúnez P, Hien TD, Kowalczyk H (1997). Parameter Sensitivity in Nonlinear Mechanics: Theory and Finite Element Computations. New York: John Wiley & Sons.

Klema VC, Laub AJ (1980). The singular value decomposition: Its computation and some applications. *IEEE Transactions on Automatic Control*, 25: 164–176.

Kristensen MH, Petersen S (2016). Choosing the appropriate sensitivity analysis method for building energy model-based investigations. *Energy and Buildings*, 130: 166–176.

Ladevèze P (1977). Nouvelle procédure d'estimation d'erreur relative à la méthode des éléments finis et applications. Publications Mathématiques et informatiques de Rennes, pp. 1–19. (in French)

Ladevèze P, Nedjar D, Reynier M (1994). Updating of finite element models using vibration tests. *AIAA Journal*, 32: 1485–1491.

Ladevèze P, Chouaki A (1999). Application of a posteriori error estimation for structural model updating. *Inverse Problems*, 15: 49–58.

Ladevèze P, Moës N, Douchin B (1999). Constitutive relation error estimators for (visco)plastic finite element analysis with softening. *Computer Methods in Applied Mechanics and Engineering*, 176: 247–264.

Ladevèze P, Pelle JP (2005). The constitutive relation error method for linear problems. In: Ling FF, Gloyna EF, Hart WH (eds), Mastering Calculations in Linear and Nonlinear Mechanics. New York: Springer. pp. 29–50.

Ladevèze P, Puel G, Deraemaeker A, Romeuf T (2006). Validation of structural dynamics models containing uncertainties. *Computer Methods in Applied Mechanics and Engineering*, 195: 373–393.

Ladevèze P, Chamoin L (2015). The constitutive relation error method: A general verification tool. In: Chamoin L, Díez P (eds), Verifying Calculations—Forty Years On. An Overview Of Classical Verification Techniques for FEM Simulations. Cham, Switzerland: Springer. pp. 59–89.

Lawson CL, Hanson RJ (1974). Solving Least Squares Problem. Englewood Cliffs, NJ, USA: Prentice-Hall,

Li X, Nassiopoulos A, Waeytens J, Chakir R (2015). A posteriori estimation of modeling error for a building thermal model. In: Proceedings of VII International Conference on Adaptive Modelling and Simulation (Admos 2015).

Li W, Tian Z, Lu Y, Fu F (2018). Stepwise calibration for residential building thermal performance model using hourly heat consumption data. *Energy and Buildings*, 181: 10–25.

Maday Y, Mula O (2013). A generalized empirical interpolation method: Application of reduced basis techniques to data assimilation. In: Brezzi F, Colli Franzone P, Gianazza U, Gilardi G (eds), Analysis and Numerics of Partial Differential Equations. Milano: Springer. pp. 221–235.

Maday Y, Mula O, Patera AT, Yano M (2015a). The generalized empirical interpolation method: stability theory on Hilbert spaces with an application to the stokes equation. *Computer Methods in Applied Mechanics and Engineering*, 287: 310–334.

Maday Y, Patera AT, Penn JD, Yano M (2015b). A parameterized-background data-weak approach to variational data assimilation: formulation, analysis, and application to acoustics. *International Journal for Numerical Methods in Engineering*, 102: 933–965.

Mangematin E, Pandraud G, Roux D (2012). Quick measurements of energy efficiency of buildings. *Comptes Rendus Physique*, 13: 383–390.

Marchand B, Chamoin L, Rey C (2016). Real-time updating of structural mechanics models using Kalman filtering, modified constitutive relation error, and proper generalized decomposition. *International Journal for Numerical Methods in Engineering*, 107: 786–810.

Marchand B, Chamoin L, Rey C (2019). Parameter identification and model updating in the context of nonlinear mechanical behaviors using a unified formulation of the modified Constitutive Relation Error concept. *Computer Methods in Applied Mechanics and Engineering*, 345: 1094–1113.

Martínez S, Erkoreka A, Eguía P, Granada E, Febrero L (2019). Energy characterization of a PASLINK test cell with a gravel covered roof using a novel methodology: Sensitivity analysis and Bayesian calibration. *Journal of Building Engineering*, 22: 1–11.

Morozov VA (1966). On the solution of functional equations by the method of regularization. Doklady Akademii Nauk SSSR, 167(3): 510–512.

Nassiopoulos A, Kuate R, Bourquin F (2014). Calibration of building thermal models using an optimal control approach. *Energy and Buildings*, 76: 81–91.

Nguyen H-M, Allix O, Feissel P (2008). A robust identification strategy for rate-dependent models in dynamics. *Inverse Problems*, 24: 065006.

Nouy A (2010). A priori model reduction through Proper Generalized Decomposition for solving time-dependent partial differential equations. *Computer Methods in Applied Mechanics and Engineering*, 199: 1603–1626.

Oden J, Prudhomme S (2002). Estimation of modeling error in computational mechanics. *Journal of Computational Physics*, 182: 496–515.

Ohlberger M, Rave S (2016). Reduced basis methods: Success, limitations and future challenges. In: Proceedings of ALGORITMY.

Papadimitriou C, Lombaert G (2012). The effect of prediction error correlation on optimal sensor placement in structural dynamics. *Mechanical Systems and Signal Processing*, 28: 105–127.

Quarteroni A, Manzoni A, Negri F (2016). Reduced Basis Methods for Partial Differential Equations. Cham, Switzerland: Springer.

Raillon L, Ghiaus C (2018). An efficient Bayesian experimental calibration of dynamic thermal models. *Energy*, 152: 818–833.

Rouchier S (2018). Solving inverse problems in building physics: An overview of guidelines for a careful and optimal use of data. *Energy and Buildings*, 166: 178–195.

Rozza G (2009). An introduction to reduced basis method for parametrized PDEs. In: Proceedings of WSPC.

Rozza G, Malik H, Demo N, Tezzele M, Girfoglio M, Stabile G, Mola A (2018). Advances in Reduced Order Methods for parametric industrial problems in computational fluid dynamics. arXiv:1811.08319.

Rubio P-B, Louf F, Chamoin L (2018). Fast model updating coupling Bayesian inference and PGD model reduction. *Computational Mechanics*, 62: 1485–1509.

Saltelli A, Tarantola S, Campolongo F (2000). Sensitivity analysis as an ingredient of modeling. *Statistical Science*, 15: 377–395.

Signorini M, Zlotnik S, Díez P (2017). Proper generalized decomposition solution of the parameterized Helmholtz problem: application to inverse geophysical problems. *International Journal for Numerical Methods in Engineering*, 109: 1085–1102.

Thébault S, Bouchié R (2018). Refinement of the ISABELE method regarding uncertainty quantification and thermal dynamics modelling. *Energy and Buildings*, 178: 182–205.

Tikhonov TN, Arsenin Y (1977). Solutions to ill-posed problems. New York: Winston-Widley.

Waeytens J, Mahfoudhi I, Chabchoub MA, Chatellier P (2017). Adjoint-based numerical method using standard engineering software for the optimal placement of chlorine sensors in drinking water networks. *Environmental Modelling and Software*, 92: 229–238.